THE PENNSYLVANIA STATE UNIVERSITY
SCHREYER HONORS COLLEGE

DEPARTMENT OF BIOCHEMISTRY AND MOLECULAR BIOLOGY

The Properties and Location of Anisosome-Forming RNA-binding Deficient TAR DNA-Binding Protein 43 Inside the Nucleus

ELI MERTICK-SYKES
SPRING 2022

A thesis
submitted in partial fulfillment
of the requirements
for a baccalaureate degree
in Biochemistry and Molecular Biology
with honors in Biochemistry and Molecular Biology

Reviewed and approved* by the following:

Xin Zhang
Professor of Chemistry
Thesis Supervisor

Song Tan
Verne M. Willaman Professor of Molecular Biology
Honors Adviser

* Electronic approvals are on file.

ABSTRACT

The accumulation of protein aggregates is a commonly displayed phenotype for patients at different stages of disease progression in neurodegenerative disorders[1]. Much research has been done to combat these disorders, with many focusing on the ability of clearing protein aggregates or preventing their formation. The discovery that many protein aggregates initially form as misfolded or phase-separated oligomers has focused research to the prevention of these early-stage formations[2,17]. TAR DNA-binding Protein 43 kDa (TDP-43) is a particular protein that has been implicated in patients with ALS; RNA-binding domain mutations that cause the protein to oligomerize and undergo liquid-liquid phase separation (LLPS) are a commonly displayed phenotype of patients with the disease[6,18,20]. These phase-separated droplets form "anisosomes" when overexpressed in mammalian cells. This project seeks to characterize the phenotypes of multiple TDP-43 mutants as a model for the study of phase-separated oligomers.

TDP-43 was expressed as a recombinant protein with an N-terminal SNAP-tag and incubated with a modified Green Fluorescent Protein that associates with the SNAP-tag. Fluorescence assays revealed a variety of anisosome phenotypes and quantified their propensities, size, and concentration. Structural analyses provided rationalizations for the formation of anisosomes but could not provide justifications for why certain mutants displayed differential phenotypes. Co-localization studies were performed using immunofluorescence of specific nuclear proteins to reveal potential protein-protein interactions. While some proteins exhibited signal overlap with TDP-43, many were statistically insignificant or were an artifact of improper procedural technique. Future localization assays should include enhanced microscopy techniques to support the existence of protein scaffolds or chaperones (if any) in the formation of anisosomes.

TABLE OF CONTENTS

LIST OF FIGURES

LIST OF TABLES

ACKNOWLEDGMENTS

I would like to thank Professor Xin Zhang for providing me the resources and space to carry out my thesis research. Additionally, I would like to thank Henry Hsiung for his guidance and training in the techniques of mammalian cell culture and fluorescence microscopy, both of which were imperative to completing this project.

Chapter 1

Introduction

The observation of liquid-liquid phase separation (LLPS) in biological systems has been known for over 150 years. LLPS is a process characterized by the existence of two separate phases (a dense phase resembling liquid droplet, and a dilute phase) from a homogeneous mixture[2]. While there are many processes and mechanisms that display phase separation, the formation of biomolecular condensates is an important one in biochemistry. In cells, membraneless organelles and biostructures are formed by LLPS, termed biomolecular condensates, and consist of proteins and nucleic acids[6]. They have many uses in gene transcription and regulation, protein regulation, signal transduction, and provide dynamic barriers for compartmentalization[2]. A prominent example of this phenomenon can be observed in the nucleolus of cells, where the assembly of ribosomes is active.

Biomolecular condensates have also been implicated to be the precursors for pathologic aggregates and other mechanisms of disease when its regulation is lost[3]. Normally these condensates exist based on specific stimuli (including cellular signaling, environmental perturbation or pathogen invasion). These condensates have been shown to form micro-reaction centers for chemical metabolism, inactivate cellular structures, and sequester endogenous or foreign macromolecules and metabolites[3,6,10]. In healthy cells and organisms, once a stimulus diminishes, condensates will dissolve. However, if the stimulus persists, it is thought that condensates could form higher-order structures and become insoluble aggregates[1,3,4,10]. This mechanistic progression seems intuitive— aggregates cannot just appear from nothing; they must have some precursor.

As many macromolecules cluster, the solubility in water will decrease as more molecules of water will be required to form a solvation shell around the macromolecules[32]. Many proteins, nonetheless, are soluble in water as a consequence of the mechanism of folding. Protein folding is most accurately thought of as a "3D-energy funnel," where the formation of thermodynamically-favorable intermediate conformations will guide the protein towards an overall energy minimum that corresponds to its native structure[33]. Several residue-residue and residue-solvent interactions are formed and disrupted during this process, and the enthalpic and entropic contributions from these bonds and conformations are the driving forces for this energetic bias. Hydrophobic residues often condense towards the inner core of a protein via the hydrophobic effect: water forms ordered shells around materials it solvates. The clustering of hydrophobic residues will combine the volumes of those residues in an additive manner, but the total solvent-exposed surface area will decrease. This leads to an overall reduction of water solvation shells, thereby increasing the disorder of the water solvent as an entropically-favorable process. This hydrophobic effect is considered one of the main driving forces of folding. As a consequence of the hydrophobic effect, hydrophilic residues will become exposed to the surface of the protein allowing their solubility in the cytoplasm and nucleus of the cell. The polar interactions with the solvent and other residues are enthalpically favorable and contribute to the folding energy funnel.

The question that may be posed is one of immediate consequence— if proteins are capable of forming extensive macromolecular structures and still be soluble, what is the basis for aggregation? Common case studies of aggregation indicate that a folding protein gets "trapped" in a local energy minimum corresponding to a misfolded conformation[34]. These misfolded conformations often have exposed hydrophobic residues and/or have increased beta structure, which may perturb the hydrophobic residues of neighboring proteins and induce their misfolding

and aggregation. This effect may become more pronounced if the protein has a mutation which disrupts the formation of the proper native structure, or if the protein is intrinsically disordered (characterized by the lack of significant ordered tertiary and secondary structure). This effect is dangerous and has significant pathologic outcomes. Many prion diseases including Creutzfeldt-Jakob and Bovine Spongiform Encephalopathy result from cytotoxic aggregates[35].

In the past decades, studies have indicated protein aggregation as the cause of many of the neurodegenerative diseases including, Huntingdon's, Amyotrophic Later Sclerosis (ALS), and Frontotemporal dementia (FTD)[1,3]. Among proteins found in the biomolecular condensates and pathologic aggregates of ALS, TAR DNA-Binding Protein 43 (TDP-43) is used as a model protein for this study.

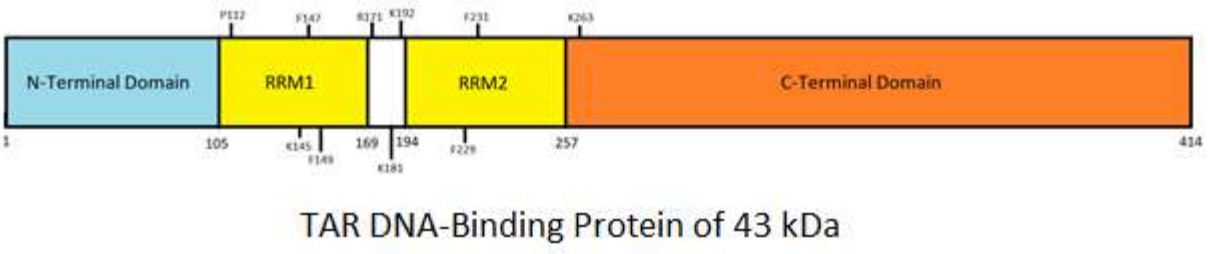

[Figure 1: Cartoon representation of the sequence of TDP-43. Labeled amino acids were selected for study.]

TDP-43 is normally localized to the nucleus and is involved in related biological processes, including regulating RNA splicing, transcription repression, and mRNA stability[8,19]. However, when placed under cellular stress, or under pathologic conditions, TDP-43 is mis-localized to the cytoplasm[11]. TDP-43 is an RNA-binding protein that consists of an N-terminal Domain (NTD), RNA-binding Domain (RBD), and C-terminal Domain (CTD) [Figure 1]. Due to the heavily dynamic nature of the protein, a complete crystal structure has not been resolved. However,

structures of these individual domains have been published. The NTD [Figure 2] has been shown to increase the tendency for a protein to undergo LLPS when covalently attached to globular proteins[5]. This suggests that the structure of the NTD likely has an important role in the mechanism of oligomerization and phase-separation. The potential for this role can be seen in its structure. The NTD adopts a dynamic and solenoid-like structure where the opposite sides carry opposite electrostatic charges[11].

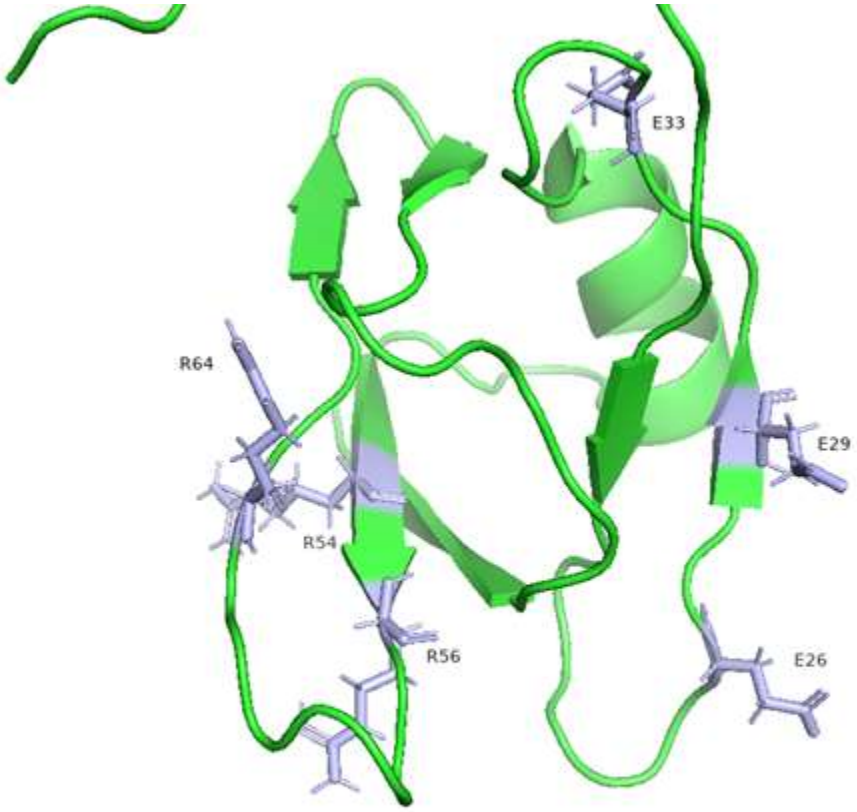

[Figure 2: NMR Structure of TDP-43 N-Terminal Domain. Selected amino acids demonstrate opposite charges on either side of the domain, allowing for dynamic solenoid-like structures to occur during oligomerization. PID: 2N4P]

This allows an ease of oligomerization to occur, as subsequent NTDs can interact with each other in an end-to-end manner. This likely assists in the reason for why TDP-43 is oligomerization and aggregation-prone[11,12]. The RBD [Figure 3] is an alpha + beta domain that binds RNA and has two major RNA recognition motifs known as RRM1 (spanning residues 105-169) and RRM2 (spanning residues 194-257)[7].

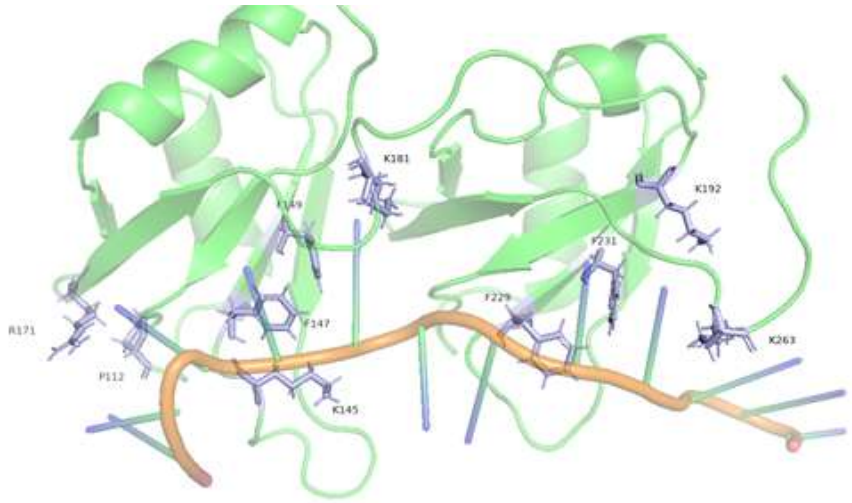

Figure 3: NMR Structure of TDP-43 RNA-Binding Domain in complex with UG-Rich RNA. The RBD contains both RRM1 and RRM2 of the sequence of TDP-43. Labeled amino acids were selected for study. PID: 4BS2

These recognition motifs consist of two alpha-helices and a 4-stranded anti-parallel beta sheet each. This domain allows for TDP-43 to perform its molecular functions because many of the RNA-binding residues are either positively charged (to interact with the negatively charged RNA phosphodiester backbone), or aromatic (to interact with the RNA bases via Pi-stacking). The CTD [Figure 4] contains a largely-intrinsically disordered region rich in asparagine, glutamine, and

phenylalanine that is essential for LLPS of TDP-43 to occur[10,11]. While most of the domain is intrinsically disordered, this domain also consists of two alpha helices.

Figure 4: NMR Structure of TDP-43 C-Terminal Domain in complex with UG-Rich RNA. PID: 2N3X

In a recent publication from the Zhang lab, an interesting hollowed spherical structure was observed when the RNA-binding ability of TDP-43 is impaired. Oligomerization of TDP-43 upon the loss of RNA-binding ability has been observed in many studies prior[23, 26-68]. This observation was confirmed by another group in 2020 and that group named these hollowed spherical condensates "anisosomes." In the paper, anisosomes are characterized as a dense outer shell with a hollow core enriched with Heat Shock Protein 70[4].

As TDP-43 becomes more relevant in its study for pathology and as a model system for LLPS, additional information surrounding anisosome formation is required. To understand the driving

forces of LLPS and the microenvironments in which it occurs, quantitative structural analyses of anisosome phenotypes were performed in cells using fluorescence microscopy. Additionally, immunofluorescence assays were utilized to visualize various other nuclear proteins to develop an understanding of the microenvironment and localizations of the anisosomes.

Chapter 2

Materials and Methods

Fluorescence microscopy is a commonly used technique in modern biochemistry, and finds many applications in determining cellular localizations, movement, or concentrations of species. Typically, fluorophores (fluorescent molecules) are conjugated to a macromolecule of interest such that it can be studied in vitro and in vivo. The microscope will shine a light of a given wavelength, and the fluorophore will be excited to an excited electronic and vibrational state. The vibrational excitation will relax, causing the release of energy through non-radiative processes, and then the electronic excited state relaxes back to the ground state by emitting energy as light with a higher wavelength than the incidental light due to the loss of energy through previous relaxation processes. Many fluorophores have been engineered such that they release energy of a specific wavelength; this can then be captured by a microscope and translated into an image that can be visualized.

Many of these fluorophores have been conjugated to secondary antibodies that recognize primary antibodies which target a specific macromolecule. This allows for the visualization of specific proteins in cells and was crucial for the immunofluorescence assays.

To characterize the anisosome phenotypes and locations, TDP-43 proteins had their coding sequence modified such that their expressed forms would contain the following mutations: K181A, K181E, R171A, P112H, K263E, K145Q/K192Q (2KQ), F147L/F149L/F229L/F231L (4FL). TDP-43 was also modified to contain a SNAP-tag infused at the C-terminus. These template sequences were then ordered from GENEWIZ, and the plasmids containing the modified TDP-43 sequences were prepared by the same company.

Yields for the ordered plasmids were too low, so the plasmids were amplified by transforming them into DH5alpha competent *E. coli* cells. The cells were thawed on ice for 10 minutes and 100 ng of plasmid was incubated with 50 μL of cells. After a 30-minute incubation on ice, the cells were heat shocked at 42°C for 30 seconds and were placed back on ice for 5 minutes. Afterwards, 950 μL of room temperature Luria Broth medium was added to the cells, and the mixture was placed in a 37°C shaking incubator at 225 rpm for 1 hour. The mixture was diluted 100-fold and then spread onto LB agar plates containing kanamycin and was finally incubated overnight at 37°C. Grown colonies were cells containing the amplified plasmid due to the plasmid containing a kanamycin-resistance gene. The amplified plasmids were then isolated using a Plasmid Midiprep protocol.

A colony of transformed DH5alpha *E. coli* cells were inoculated in a 100 mL culture of LB medium and were shaken for 16 hours. The cells were pelleted by centrifugation at 4000 xg for 10 minutes, and the pellets were resuspended in 3 mL resuspension solution (containing RNase A). Then, 3mL of cell lysis buffer was added, and the mixture was mixed. After a 5-minute incubation at room temperature, 3 mL precipitation buffer was added and gently shaken, followed by a 3min incubation at room temperature to allow precipitate to form. The lysate was centrifuged at 10000 xg for 10 minutes and the supernatant was loaded onto a DNA-binding column and was flashed through the column by centrifugation at 10000 xg. The flow-through was discarded and the column was washed twice with wash buffer. The column as then washed with 4 mL wash buffer containing isopropanol. The DNA was eluted with 2 mL distilled water.

Human Embryonic Kidney (HEK293T) cells were grown for 24 hours at 37°C on microscope coverslips in 6-well plates with 2 mL Dulbecco's Modified Eagle Medium containing 10% Fetal Bovine Serum and 1% Penicillin-Streptomycin-Glutamine. TDP-43 mutant plasmids were then

transfected into the HEK293T cells using lipofection carried out by Opti-MEM and X-treme gene 9 transfection reagent. Lipofection mixture included TDP-43 plasmid (1000 ng), Opti-MEM media (100 μL), and X-treme Gene 9 transfection reagent (2 μL per 1000 ng plasmid). After a 24-hour incubation period at 37°C, cell media was replaced to promote translation of plasmids, and cells were stained with Oregon green fluorescent protein (final well concentration of 0.5 μM). After an additional 24-hour incubation at 37°C, cells were fixed with 4% formaldehyde in 1X PBS solution. Each well was washed 3 times with 1X PBS solution for 5 minutes while lightly shaken. After washing with 1X PBS solution, an immunofluorescence staining protocol was followed (S1).

Fixed HEK293T cells transfected with plasmid were incubated with 0.5% Triton X-100 in 1X PBS solution for 10 minutes at room temperature. After 3 washing steps with 1X PBS at 5 minutes each, the cells were incubated with 3% Bovine Serum Albumin in 1X PBS solution for 1 hour at room temperature to prevent non-specific antibody binding. Primary antibodies [Table 1] were utilized to target specific endogenous proteins in eukaryotic nuclei. The primary antibodies were prepared in 3% BSA solution in a 1:200, 1:300, or 1:500 dilution. The primary antibody solution was then incubated with the coverslips covered in HEK293T cells for 1 hour at room temperature. After washing steps, secondary antibodies targeting the primary antibodies were prepared in 3% BSA solution in a 1:300 or 1:500 dilution. Secondary antibody solution was incubated with the cell-covered cover slips for 1 hour in the dark at room temperature. After washing steps, the microscope coverslips were prepared on microscope slides and were then imaged.

[Table 1: Overview of the primary antibodies used and their respective conjugated secondary antibody.]

Primary Antibody	Primary Antibody Source	Primary Antibody Target	Dilution in 3% BSA Solution	Conjugated Secondary Antibody	Secondary Antibody Source	Secondary Antibody Target	Dilution in 3% BSA Solution
Anti-SC35 Monoclonal Antibody (ab204916)	Rabbit	SC-35 Protein	1:200	Alexa Fluor™ Plus 594 Polyclonal Antibody (AB_2762824)	Goat	Rabbit IgG	1:300
Anti-PML Monoclonal Antibody (ab179466)	Rabbit	PML Protein	1:300	Alexa Fluor™ Plus 568 (AB_10563566)	Goat	Rabbit IgG	1:500
Anti-SFPQ Monoclonal Antibody (ab177149)	Rabbit	SFPQ Protein	1:500	Alexa Fluor™ Plus 568 (AB_10563566)	Goat	Rabbit IgG	1:500

The fluorescence assays were all performed in vitro with immortalized mammalian cell lines of Human Embryonic Kidney cells (HEK293T). HEK293T cells were allowed to grow for 24 hours after passaging and transfection mixtures were prepared according to a lipofection protocol; a mixture containing TDP-43 plasmid (1000ng), Opti-MEM media (100ul), and X-treme Gene 9 transfection reagent (2 μL per 1000ng). Mixtures were incubated in the dark for 30 minutes and were then incubated 0.5 μM of another plasmid containing OG-GFP in the cell cultures for 24 hours. Cells were then fixed with 4% formaldehyde in 1X PBS solution and were then imaged or were further prepared for immunofluorescence study.

Images were all taken on a ZEISS Axio Observer microscope and processed using ImageJ (an open-source Java-based image processing program). Anisosome phenotypes were measured using this program: anisosome size was measured using measuring tools within the program, and propensities were measured by counting the anisosomes detected in the image.

Utilizing the technique of fluorescence microscopy, TDP-43 mutants were conjugated with GFP to allow for direct visualization in the cell. However, several complications were present in this assay. Firstly, the fluorescence microscope was useful for general localization studies, but the resolution only allowed for a 10 μm scale. Additionally, the possibility for oversaturation of fluorescent signals can lead to inflated measurements. As such, precise measurements of anisosome diameters are difficult to achieve. However, the microscope allows to control the exposure and intensity of a fluorescent signal, which alleviates the oversaturation obstacle. Additionally, TDP-43 signals in areas of higher oligomerization will experience a stronger and broader signal because each TDP-43 molecule is conjugated to a fluorophore, leading to an additive increase in diameter. Therefore, while fluorescence microscopy does not guarantee exactness in the measured anisosome sizes, it will still provide distinct method for determining granules that have experienced higher oligomerization. For future experiments, the use of confocal microscopy or SEM would prove highly beneficial.

Chapter 3

Results

Study of RNA-Binding Affinity and Anisosome Size Correlation

With recent developments in the study of liquid-liquid phase separation, the relationship between RNA-binding affinity and anisosome formation has been discussed, but not quantified. Several mutations when expressed *in vitro* do not display the same anisosome phenotype as other mutants. Some display very large and robust anisosomes, but others form miniscule and nearly diffuse anisosomes. Perhaps the phenotypes of the anisosomes are directly correlated to the RNA-binding affinity. To quantify a possible link between affinity and anisosome phenotype (propensity, diameter, quantity in cell), the well-established techniques of fluorescence microscopy, recombinant proteins, and tissue culture were utilized to characterize the anisosomes in live cells. Anisosome propensity, diameter, and quantity were chosen as indicators of anisosome phenotypes due to the nature of oligomerization. As diameter increases, the degree of oligomerization is higher because more TDP-43 molecules must be present to form a larger anisosome. The propensity of anisosome formation is defined here as the ratio of the number of cells with an anisosome phenotype to the total number of cells that were transfected. This value gives an indication of a mutation's ability to undergo anisosome formation relative to other mutations. Finally, the quantity of anisosomes is the average number of anisosomes present in cells.

Seven mutations were utilized to study the correlation of binding affinity and anisosome size: K181A, K181E, R171A, P112H, K263E, K145Q/K192Q (2KQ), F147L/F149L/F229L/F231L (4FL). These mutations were selected as they have all been present in TDP-43 proteins from patients with ALS and have also been used in other groups for research on TDP-43 phase

separation[4]. The template sequences of TDP-43 (including the mutants) were ordered online, and plasmids of the mutants were generated via restriction cloning. The ordered sequences were amplified using PCR, which was then purified and transformed into DH5alpha E. *coli* cells for further amplification. Amplified plasmid DNA was then purified using Midi-prep protocols and sequenced to verify success of amplification. Mutants of TDP-43 were fused with a SNAP-tag at the C-terminus. These SNAP-tags allow complexation with fluorophore ligands to produce a fluorescent signal.

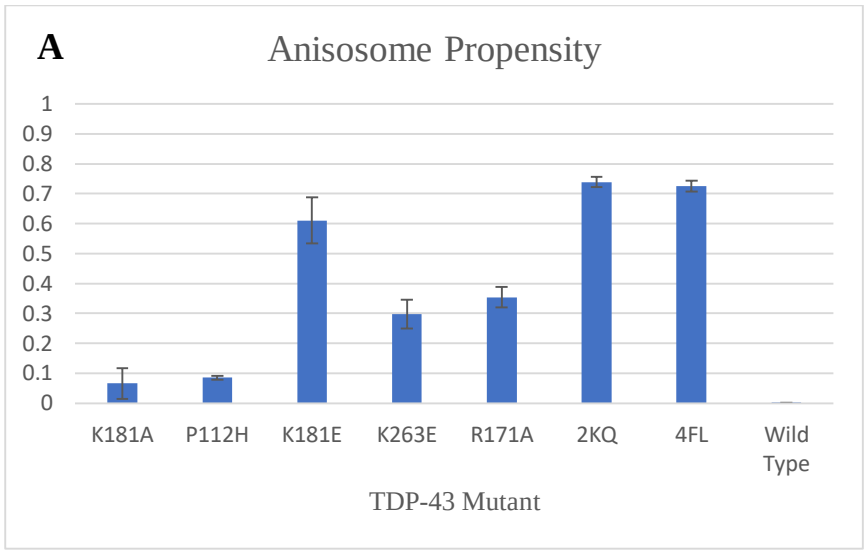
A
Anisosome Propensity
1
0.9
0.8
0.7
0.6
0.5
0.4
0.3
0.2
0.1
0
K181A
P112H
K181E
K263E
R171A
2KQ
4FL
Wild Type
TDP-43 Mutant

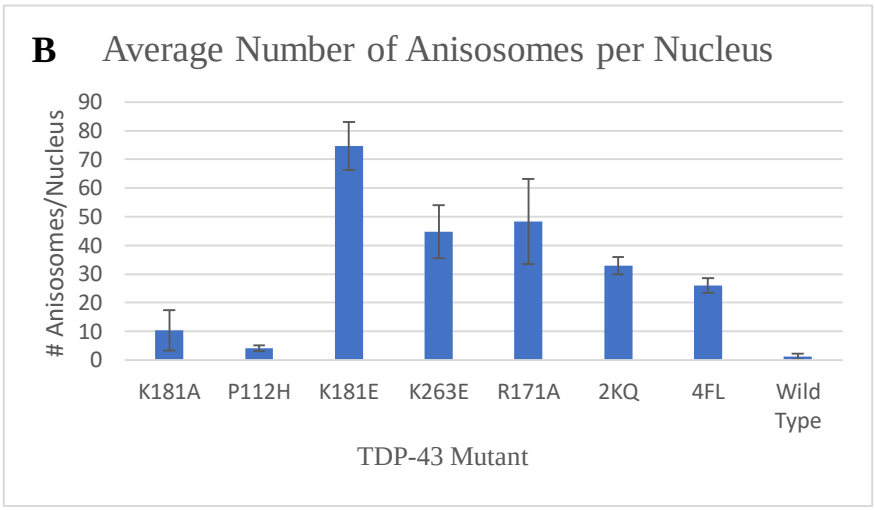
B
Average Number of Anisosomes per Nucleus
Anisosomes/Nucleus
90
80
70
60
50
40
30
20
10
0
K181A
P112H
K181E
K263E
R171A
2KQ
4FL
Wild Type
TDP-43 Mutant

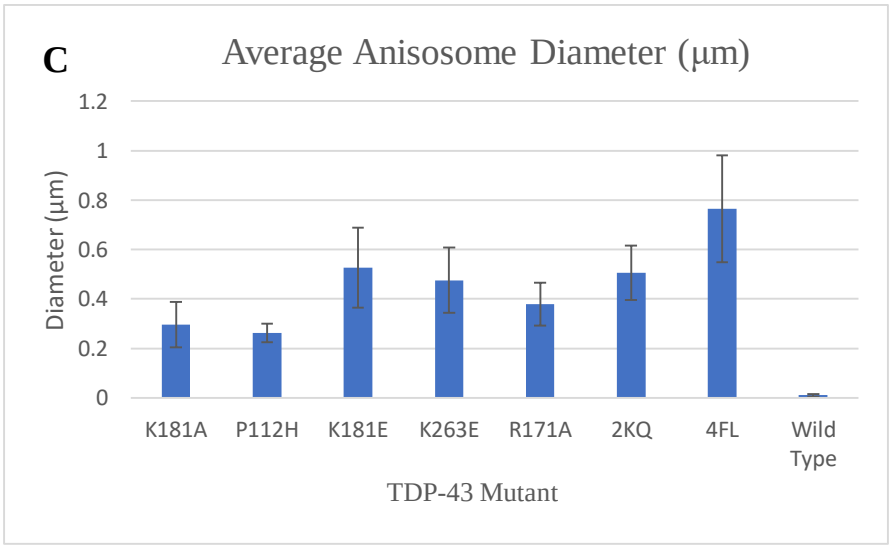
C
Average Anisosome Diameter (μm)
Diameter (μm)
1.2
1
0.8
0.6
0.4
0.2
0
K181A
P112H
K181E
K263E
R171A
2KQ
4FL
Wild Type
TDP-43 Mutant

*[Figure 5: A. Graphical representation of mean proportion of transfected cells displaying anisosome phenotypes to all transfected cells in the population. B. Average number of displayed anisosomes per cell, determined by taking average of three separate cells. C. Calculated average diameter of anisosomes displayed by each mutant. *Note- the wild-type data for anisosome propensity and average diameter was very invariable, resulting in small margins of error that do not display well on the graphs.]*

The overall results are demonstrated in Figure 5. All the mutants were capable of forming anisosomes, but the phenotypes varied widely. Anisosome phenotypes rely upon the use of fluorescence microscopy, which does not provide structural or chemical data. It is known that TDP-43 must oligomerize to phase separate, so it cannot be said with absolute certainty that the phenotypes observed were phase-separated. Some of the signals may be insoluble aggregates, or oligomers that have not yet undergone LLPS. Despite this drawback, this study aims to characterize the degree of oligomerization, and so the state of phase-separation does not matter. Anisosomes are generally characterized by punctate GFP signals caused by the oligomerization of TDP-43. Contrastingly, wild-type TDP-43 signal is largely diffuse [Figure 6]. K181A and P112H overall displayed similar anisosome phenotypes— and both closely resembled the wild-type TDP-43 [Figure 7].

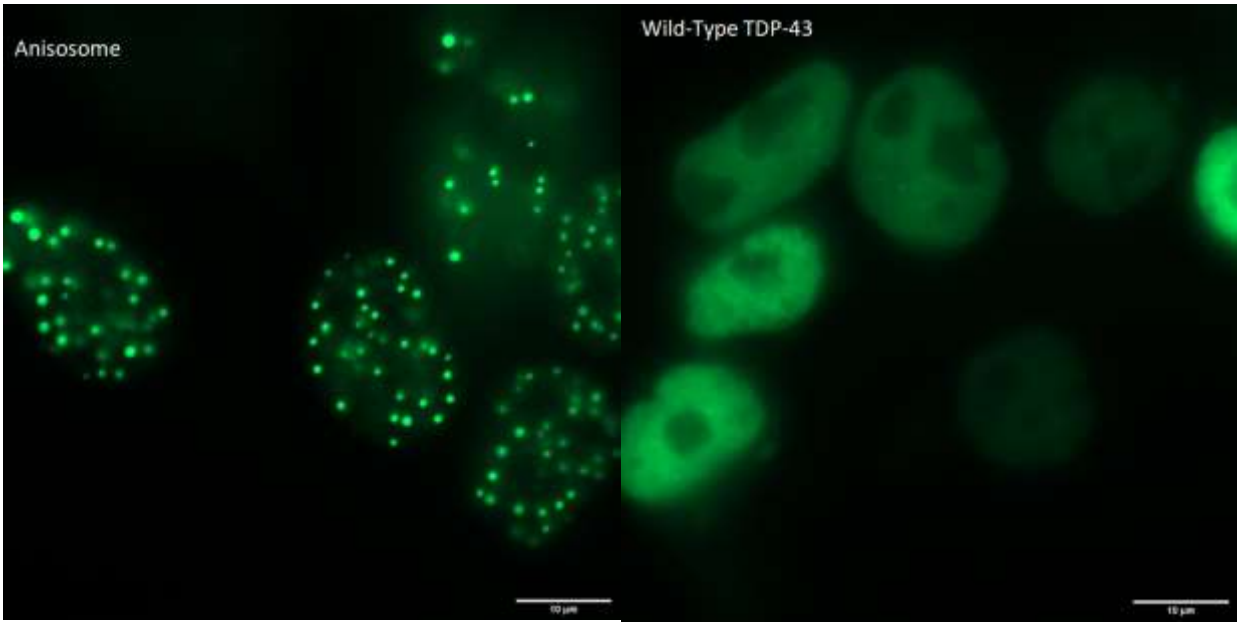

[Figure 6: Left- General anisosome GFP signal phenotype (K145Q/K192Q). Right- Wild-Type TDP-43 GFP signal phenotype. 10 μm scale. GFP were excited at 488nm, and signals were captured at 509nm at 20% light intensity and 150ms exposure time.]

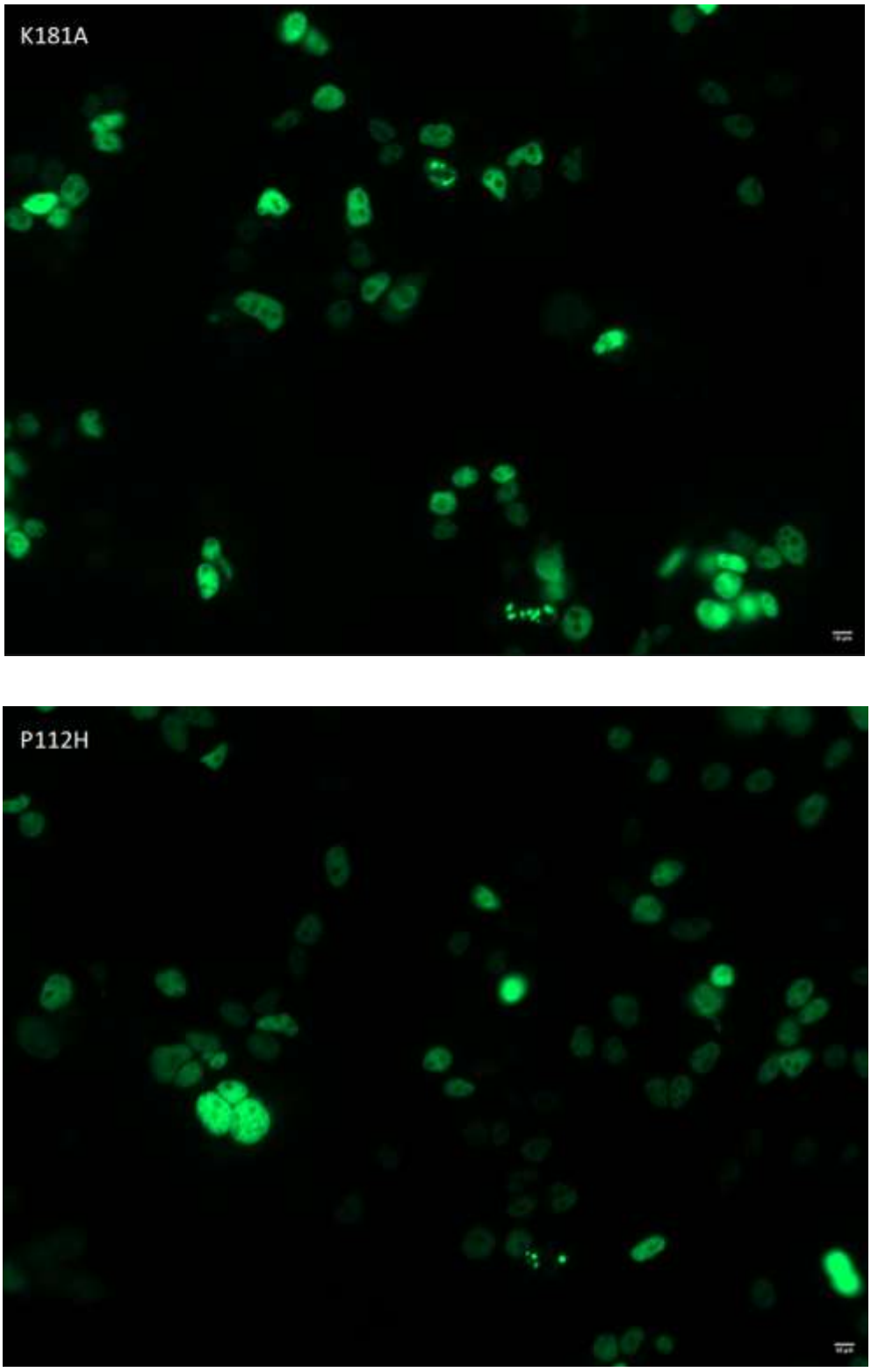

[Figure 7: Top- K181A anisosome phenotype. Bottom- P112H anisosome phenotype. 10 μm scale. GFP were excited at 488nm, and signals were captured at 509nm at 20% light intensity and 150ms exposure time.]

Additionally, R171A [Fig. 8] exhibited an overall increase in anisosome propensity and number in comparison to the wild-type K181A and P112H. However, the anisosomes formed by R171A oligomerization were about the same diameter as the previous two mutants. Following this result, the mutants of K181E [Fig. 9] and K263E [Fig. 10] were tested, as they occupy structurally similar areas of the protein to each other. Interestingly, despite this similarity, they only demonstrated similar diameter size. Their propensities and differed by nearly a factor of 2, with K181E exhibiting the higher propensity.

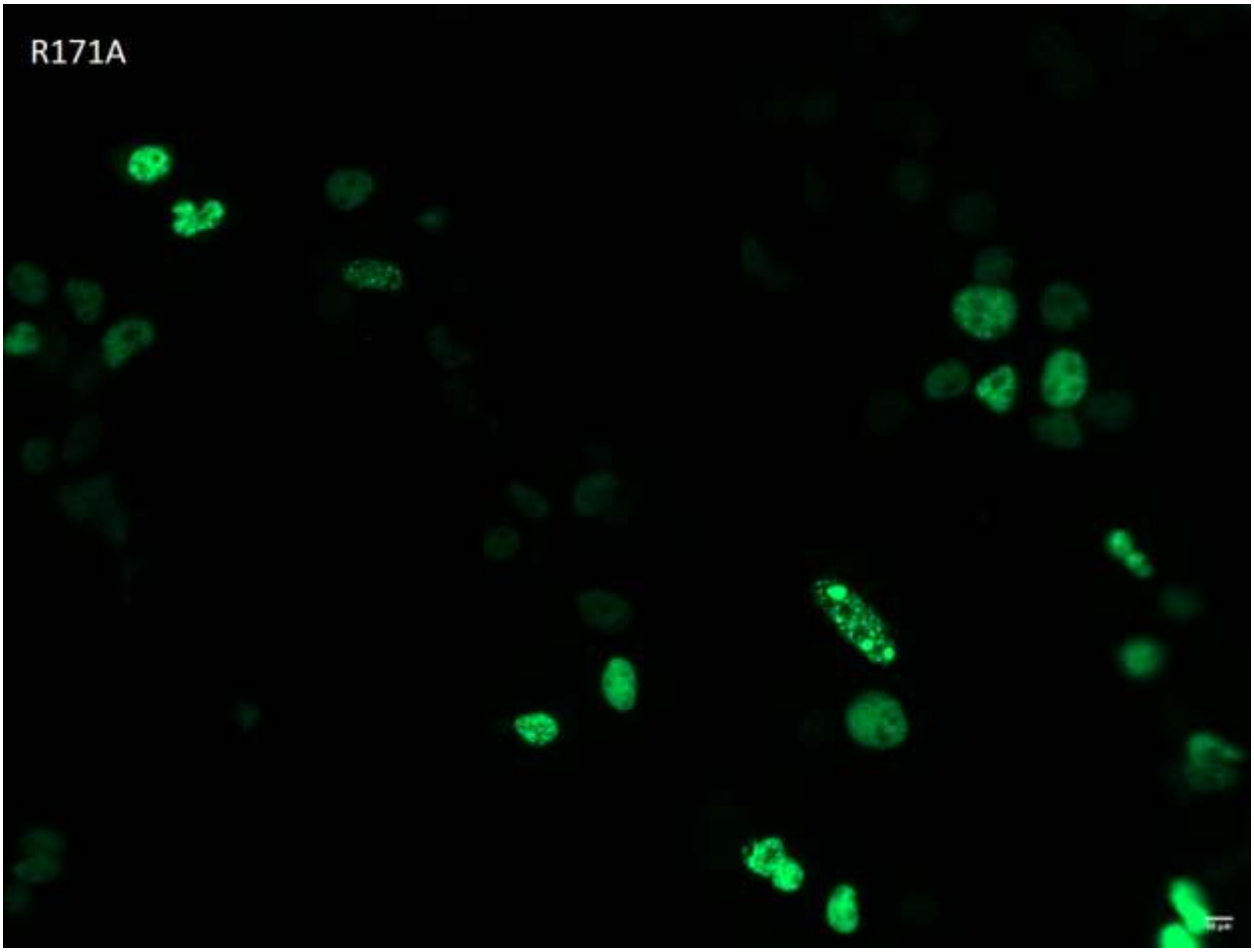

[Figure 8: R171A GFP signal. 10 μm scale. GFP were excited at 488nm, and signals were captured at 509nm at 20% light intensity and 150ms exposure time.]

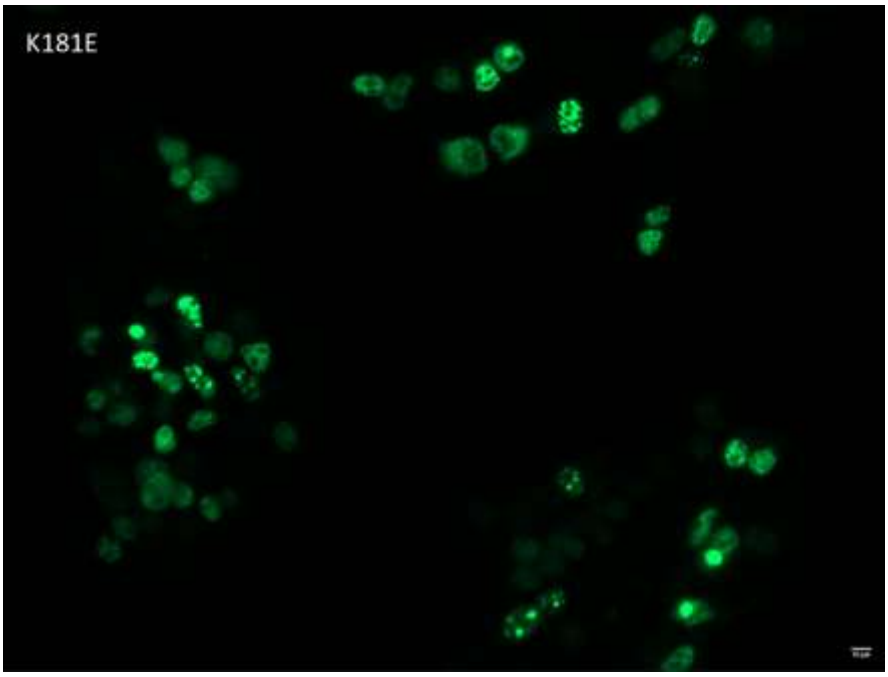

[Figure 9: K181E GFP signal. 10 μm scale. GFP were excited at 488nm, and signals were captured at 509nm at 20% light intensity and 150ms exposure time.]

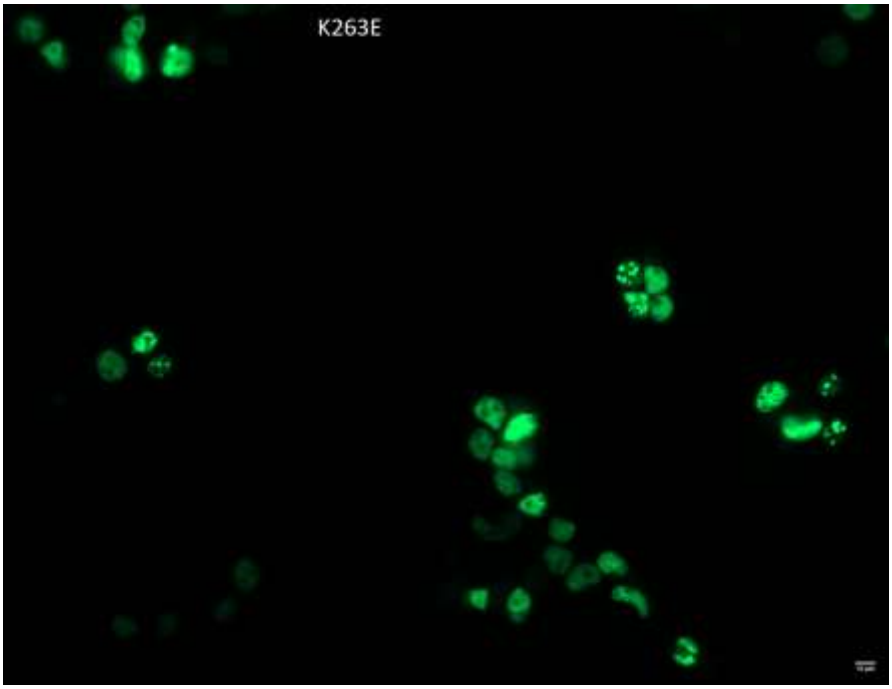

[Figure 10: K263E GFP signal. 10 μm scale. GFP were excited at 488nm, and signals were captured at 509nm at 20% light intensity and 150ms exposure time.]

The last two mutants, K145Q/K192Q [Fig. 11] and F147L/F149L/F229L/F231L [Fig. 12] demonstrated the most punctate anisosome phenotypes. Their anisosome propensities were almost identical and higher than any other mutant tested. Additionally, their diameters were much larger than the other mutants, except for K181E. An interesting result is that the total number of anisosomes formed in the cells were lower than the other moderately-high propensity mutants. A likely explanation is that since anisosomes form through oligomerization, and there exists a finite number of TDP-43 proteins in the cell, extensive oligomer size will decrease the number of TDP-43 proteins available to form new anisosomes.

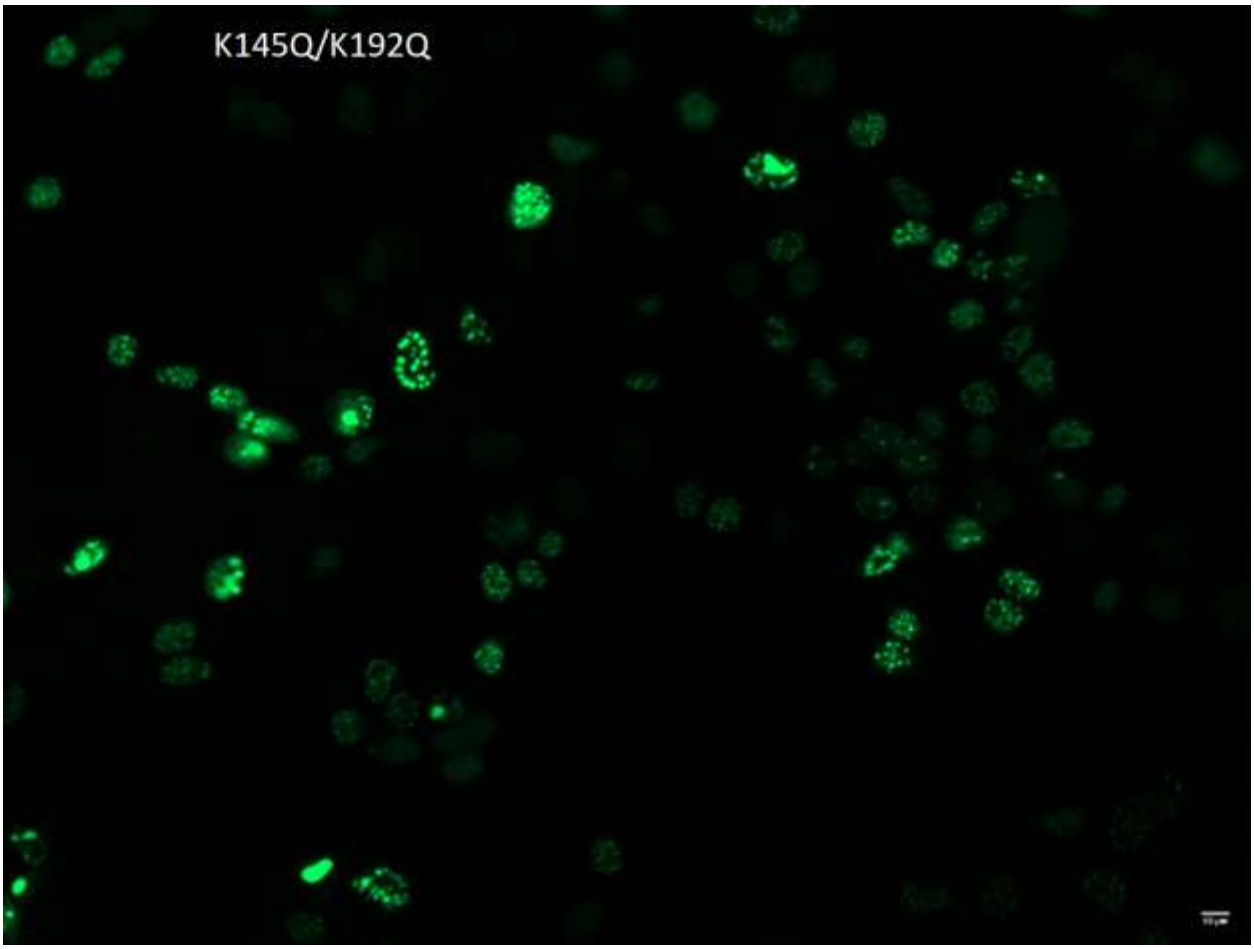

[Figure 11: K145Q/K192Q GFP signal. 10 μm scale. GFP were excited at 488nm, and signals were captured at 509nm at 20% light intensity and 150ms exposure time.]

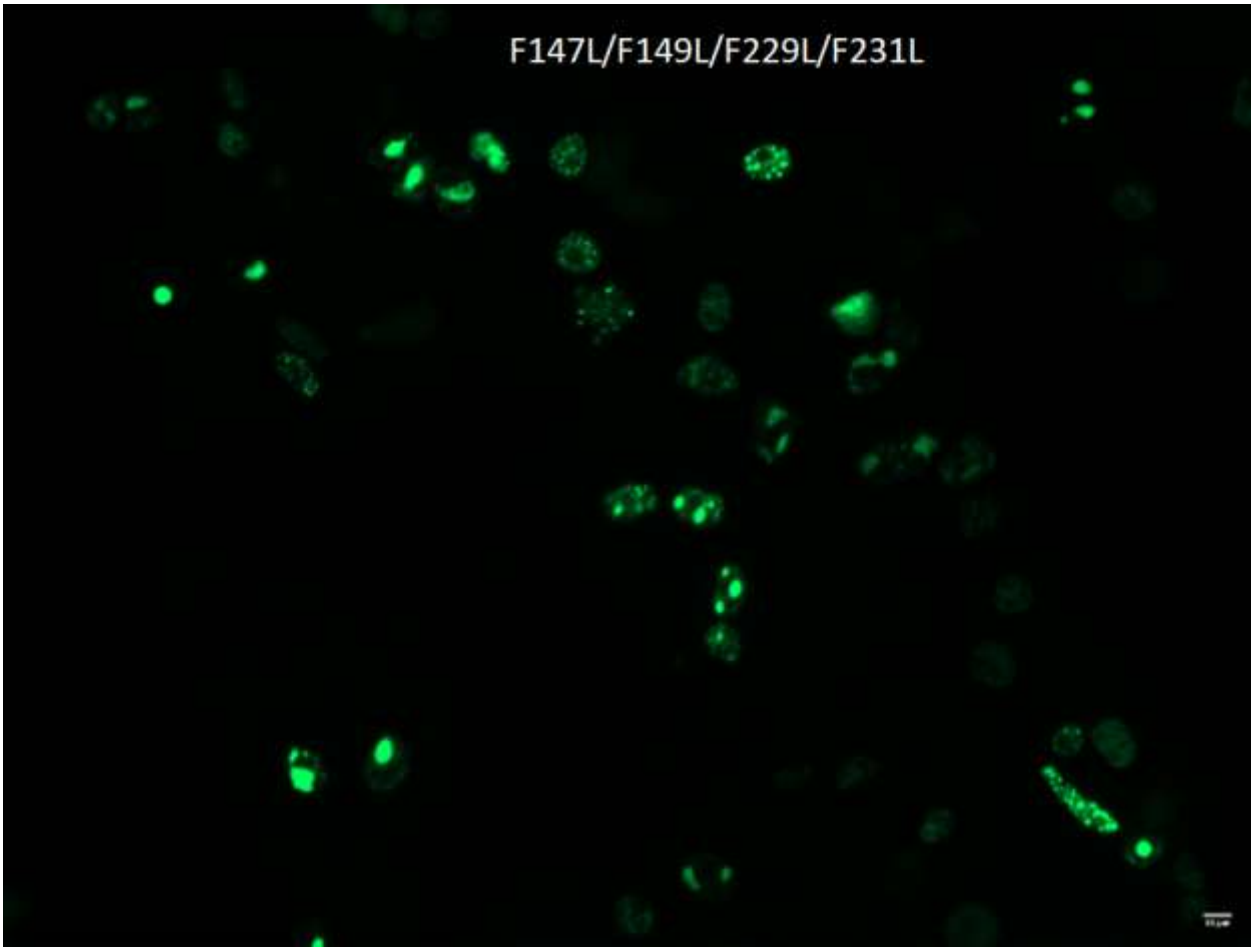

[Figure 12: F147L/F149L/F229L/F231L GFP signal. 10 μm scale. GFP were excited at 488nm, and signals were captured at 509nm at 20% light intensity and 150ms exposure time.]

To test anisosome propensity, three nuclei of three separate photos were counted for the number of anisosomes per nucleus of each mutant. The average anisosome diameter of each mutant was calculated by directly measuring the diameter of each fluorescent signal of the anisosomes in five different cells each using the program ImageJ. In these experiments, the limitations of fluorescence microscopy were quite prevalent. Fluorescent signals have a risk of oversaturation and may lead to inflated diameter readings because of signal bleeding. To combat this, all fluorescence levels were brought below saturation.

Co-localization studies

To identify any possible molecular scaffolds, chaperones, or proteins in complex with TDP-43 oligomers, the study of the localization of TDP-43 mutants with endogenous nuclear proteins was conducted using immunofluorescence. Any nuclear proteins that have significant overlap with TDP-43 would likely be in complex or associated with the TDP-43 anisosomes. Sporadic and diffuse signals of the nuclear proteins is indicative of little association present between the two proteins.

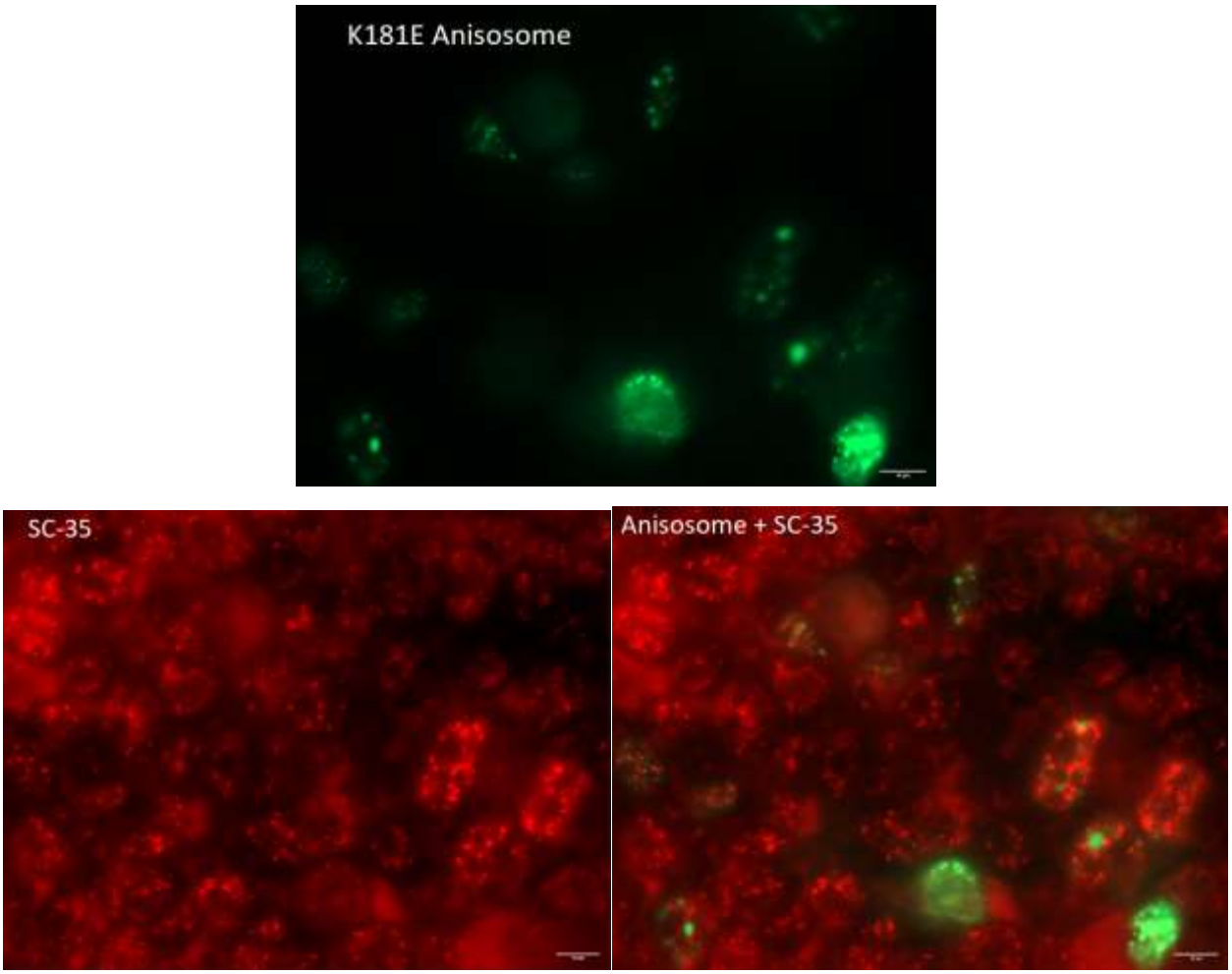

[Figure 13: TDP-43 Anisosome (K181E) Localization with SC-35. (Top) TDP-43 conjugated with Green Fluorescent Protein. (Bottom left) SC-35 stained with Alexa Fluor™ 594 secondary antibodies. (Bottom Right) Overlay of both green and red signals. GFP 20% intensity, Exposure 150ms. AF594 75% intensity, Exposure 150ms]

The first nuclear protein chosen was SC35 [Figure 13]. SC35 is a splicing factor that is relatively abundant in the nucleus. Splicing factors commonly form complexes with others during transcription; perhaps an association would occur between SC35 and TDP-43. However, the green and red fluorescent signals did not display any significant overlap, even across various anisosome phenotypes. Although the anisosomes would localize alongside some SC35 bodies, the overall lack of overlap associated with these proteins indicates that there is likely little structural association between the two. The second nuclear protein chosen was PML [Fig. 14]. Promyelocytic leukemia protein is a tumor suppressor protein that has been implicated in the assembly of several nuclear structures that bind to chromatin. This protein appeared to have some significant overlap with TDP-43, but less than 60% of TDP-43 signals were associated with a PML body. Finally, a third nuclear protein visualized: Splicing Factor Proline and Glutamine-Rich. SFPQ is another splicing factor in the nucleus, and because splicing factors tend to interact, it was believed to be a reasonable candidate. The signals of these SFPQ and TDP-43 initially had distinct fluorescent overlap demonstrated by the signals [Fig. 15]. However, future experiments with differing antibody concentrations did not produce the same result [Fig. 16]. Instead of displaying distinct and unique overlap, there was a diffuse signal of SFPQ throughout the cell. This observation implicated that there may be a concentration dependence of the displayed phenotype. Perhaps higher concentrations of secondary antibodies caused clumps to form and produce signals that may not otherwise have been present.

Due to external factors regarding the lab and the SARS-CoV-2 pandemic, several beneficial assays could not be performed. Binding assays of each of the mutants would have provided additional quantifiable parameters for anisosome phenotype. Further colocalization studies could not be performed to test further concentration dependence of the results of other nuclear proteins.

Additionally, due to the lack of secondary antibody supply, multi-body overlap studies could not be performed to display a more complete picture of TDP-43 localization. The polyclonal secondary antibodies used were anti-IgG, meaning that even if two separate secondary antibodies were used to target the primary antibodies, there would be no way to differentiate the signals as they would bind to either primary antibody's IgG domain. To improve this, secondary antibodies would need to be purchased that are anti to the specific primary antibodies used. Future experiments with allocated time and resources will provide beneficial supporting characterizations of the mutants studied here.

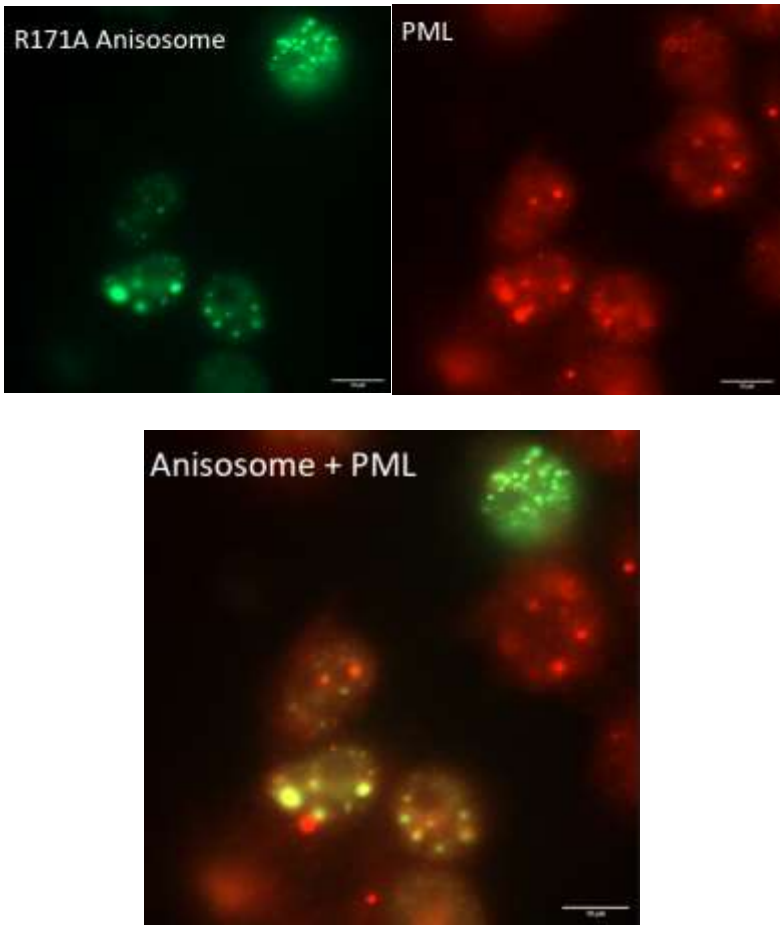

[Figure 14: TDP-43 Anisosome (R171A) Localization with PML. (Left) TDP-43 conjugated with Green Fluorescent Protein. (Middle) SC-35 stained with Alexa Fluor™ 568. (Right) Overlay of both green and red signals. GFP 20% intensity, 150ms. Red 75% intensity, 300ms]

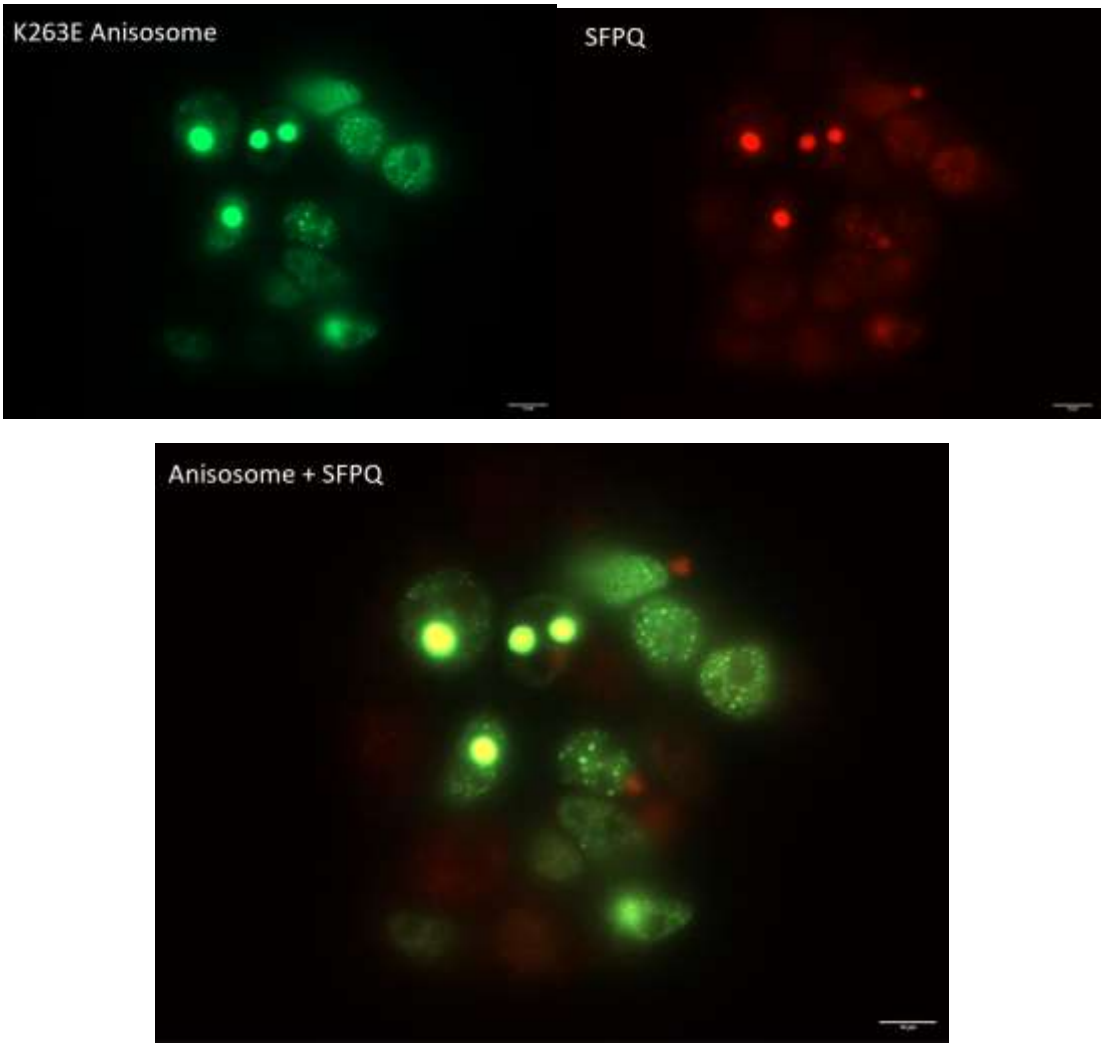

[Figure 15: TDP-43 Anisosome (K263E) Localization with SFPQ. (Left) TDP-43 conjugated with Green Fluorescent Protein. (Right) SFPQ stained with Alexa Fluor™ 568. (Bottom) Overlay of both green and red signals. GFP 20% intensity, 50ms. Red 75% intensity, 300ms]

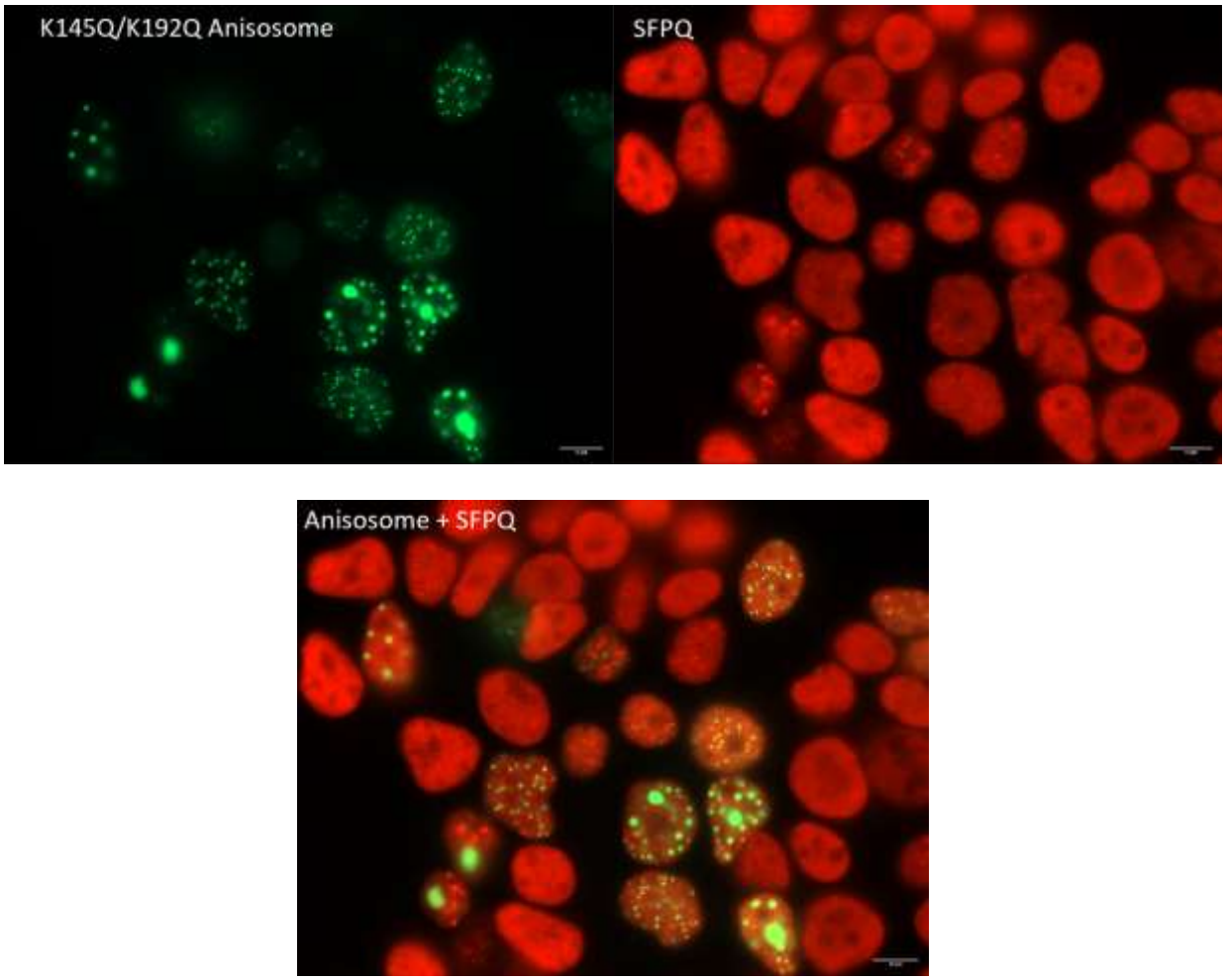

[Figure 16: TDP-43 Anisosome (K145Q/K192Q) Localization with SFPQ. (Left) TDP-43 conjugated with Green Fluorescent Protein. (Right) SFPQ stained with AlexaFluor 568. (Bot) Overlay of both green and red signals. GFP 20% intensity, 150ms. Red 75% intensity, 200ms]

Chapter 4

Discussion

The correlation of anisosome size and propensity has been demonstrated with the fluorescence assays above. For a rigorous understanding of these correlations, an analysis of the structure of TDP-43 may provide insight for the mechanisms and driving forces behind oligomerization and liquid-liquid phase separation.

As RNA-binding affinity is reduced, the propensity for anisosome formation generally increases. This is because RNA stabilizes the structure of TDP-43[27,28], likely through thermodynamic stabilization (the formation of new, energetically favorable interactions). Specifically, the binding of RNA to TDP-43 provides enthalpically favorable interactions that allow for the secondary structure to form, even though the protein entropy contribution becomes less favorable. Whenever TDP-43 loses its ability to bind RNA, in the absence of other TDP-43/miscellaneous proteins, TDP-43 likely adopts a heavily disordered state as the most favorable. Thus, when placed in high concentration solution of TDP-43 without sufficient RNA-binding, it likely finds other enthalpically favorable interactions with other TDP-43 proteins until an energy minimum is reached.

The mutations of K145Q and K192Q are an acetylation mimic found in patients with ALS. When K145/K192 are mutated to K145Q/K192Q in tandem, the binding affinity for RNA severely decreases. This has been confirmed by cross-linked immunoprecipitation assays and absorbance readings[7]. K145 forms a salt-bridge with the phosphodiester backbone of RNA [Figure 17]. This interaction is enthalpically favorable, as the positive charge of lysine and the negative charge of the backbone forms a favorable interaction. When mutated, this electrostatic interaction no longer

occurs, and severely inhibits the ability of TDP-43 to bind RNA. While structures of TDP-43 oligomers have not been published, an hypothesis may be that this mutation exposes previously-hidden binding sites that allow for the formation of more enthalpically favorable interactions when the salt-bridge is lost— leading to oligomerization.

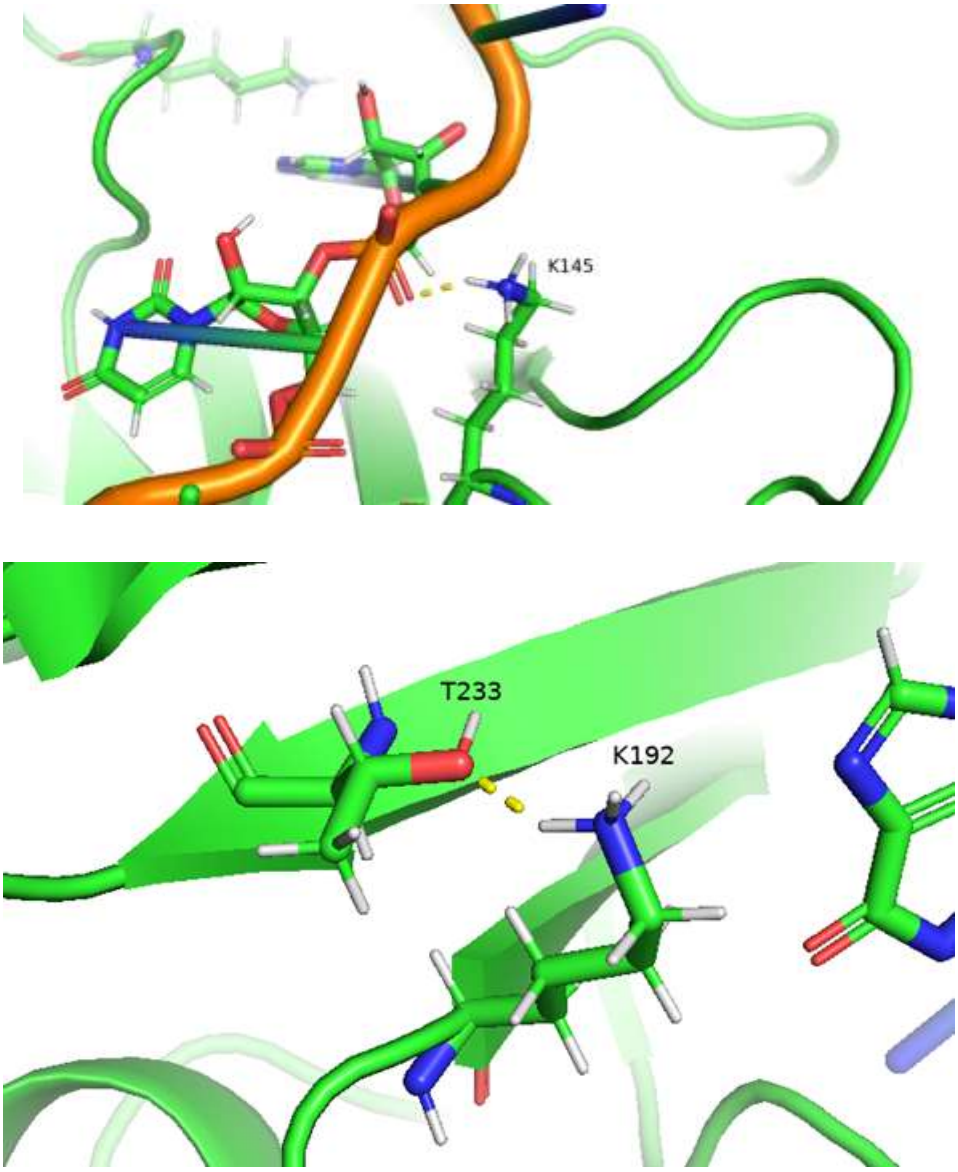

[Figure 17: Top- K145 forming a salt-bridge with the RNA phosphodiester backbone. Bottom- K192 forming a hydrogen bond with T233 of neighboring beta-sheet. PID: 4BS2]

Interestingly, K192 does not form a salt-bridge, but rather it forms a hydrogen bond with T233 [Fig. 17], a residue of a nearby beta-sheet. While the hydrogen bond to the beta-sheet would decrease the conformational entropy of the protein (an unfavorable result), it may lock the conformation of the protein such that it forms many enthalpically favorable interactions with RNA, offsetting the unfavorable entropy change. The loss of this hydrogen bond may cause a conformational change that leads to oligomerization in an attempt to form more stable interactions. Consistent with these hypotheses, the literature suggests that K145Q/K192Q tandem mutations induce a conformational change preventing RNA-binding[4]. However, no structural studies were performed, nor were binding assays performed for K192Q alone, so it is yet to be confirmed whether K192 plays a vital role in the structural stability of TDP-43— although the current evidence suggests it does.

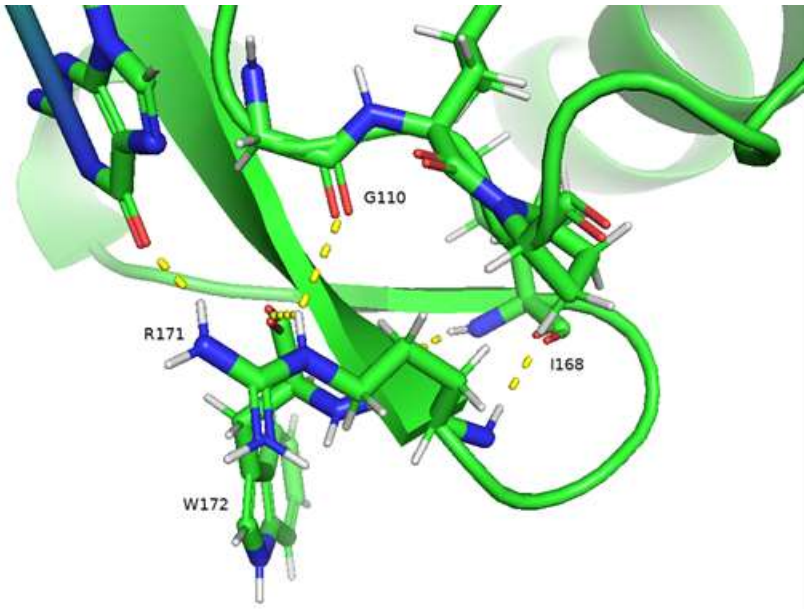

[Figure 18: R171 forming a hydrogen bond with an RNA base, a hydrogen-bond with W172, G110 backbone carbonyl, and I168 backbone carbonyl. PID: 4BS2]

Another mutation commonly present in pathology is R171A. R171 hydrogen-bonds to nucleotide bases and works alongside W113 (which base-stacks with nucleotide bases) to form interactions with nucleic acids [Fig. 18][13]. Both interactions are enthalpically favorable. Wild-type TDP-43 has a binding affinity for RNA of K_d = 20.6 +/-1.8nM and R171A has a K_d of 124.2 +/-12.7nM[13]. The loss of the donating hydrogen causes the enthalpically favorable interaction to cease. Like the K145Q/K192Q mutations, this mutation likely leads to oligomerization because TDP-43 seeks to gain higher stability by oligomerizing with itself and form favorable interactions to decrease the enthalpy.

A peculiar mutation that causes RNA-binding deficiency is K181E. K181 is a lysine residue that lies in between RRM1 and RRM2, with its exact location closer to RRM1. K181 lies within a pocket-like cavity where a nucleotide base is positioned nearby [Fig. 19].

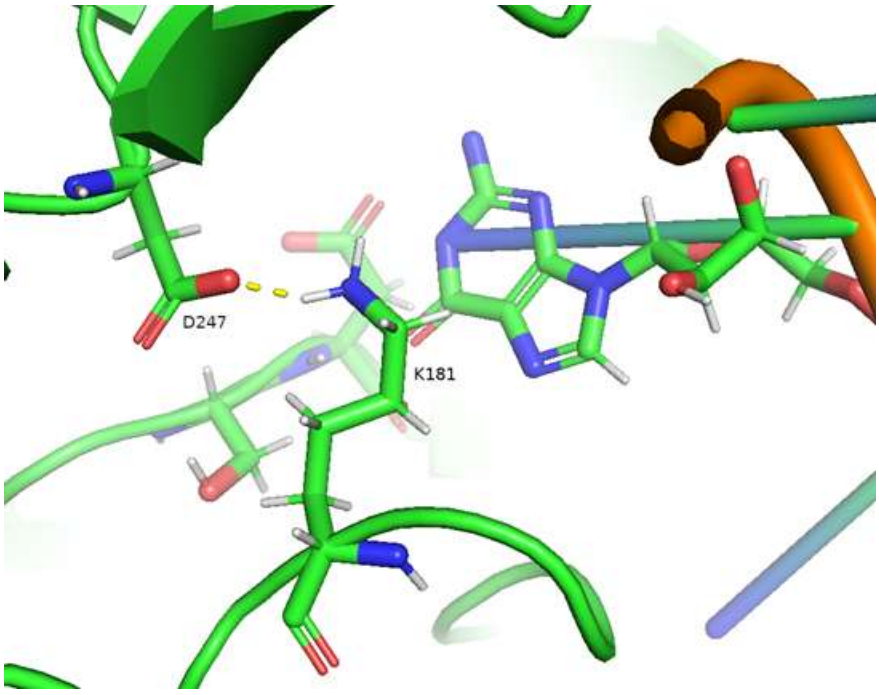

[Figure 19: K181 forming a salt-bridge with D247 side-chain carboxylate. K181 also lays near a guanine nucleotide. PID: 4BS2]

Circular dichroism and 2D HSQC-NMR experiments have supported that the introduction of K181E does not introduce a conformational change[14]. The K_d of wild-type TDP-43 was measured for UG-rich RNA against the K181E mutant. The wild type exhibited a K_d of 3.2 +/-0.9nM, but K181E exhibited a K_d of 2.5 +/-0.4uM— an almost 1000-fold increase[14]. It is quite evident that K181E has a severely inhibited ability to bind RNA. An hypothesis may be that this reduced affinity is due to electrostatic repulsion. While K181 does not appear to interact with the RNA backbone, the nucleotide bases it interacts with have tend to have carbonyl oxygens (displaying partial electronegative charges) in close proximity to K181. When this residue is mutated to glutamate (displaying a negative charge), it becomes repulsed by D247 and subsequently repels the nucleotide base. This is further supported by the results of this thesis and the study showing that the K181A mutation does not have a high propensity to form anisosomes or aggregates[12]. Alanine does not carry any charge, so electrostatic repulsion is unlikely to occur. The evidence that a conformational change does not occur with this mutation suggests a hypothesis that the lack of complexation with RNA could expose residues on TDP-43 that are prone to oligomerization by forming enthalpically favorable interactions. This is supported by co-immunoprecipitation assays displaying mutant TDP-43 in aggregates with wild-type endogenous TDP-43[14]. However, further structural studies must be performed for confirmation.

It has been found that 4FL has a 70% loss of binding affinity for RNA, while 2KQ had a 50-65% loss of binding[7]. Structural analysis of 4FL demonstrated very few polar contacts made with RNA [Fig. 20]. However, PyMOL does not discern aromatic pi-stacking interactions that have been shown to be present in these residues. The residues with the most conceivable interactions with RNA were F149 and F231; both were in structurally similar regions of the protein. Although the 4FL mutant has not had its binding affinity quantified as, there is a method to approximate it. A

paper demonstrated the K_d for F147L to be 71.2+/- 1.4nM and F149L to be 86.2 +/-7.7 nM[13]. In comparison, the wild-type had a K_d of 20.6+/- 1.8nM. It can therefore be extrapolated that these two mutations in tandem with each other will have a lower binding affinity, especially when in existence alongside their structural counterparts, F229 and F231.

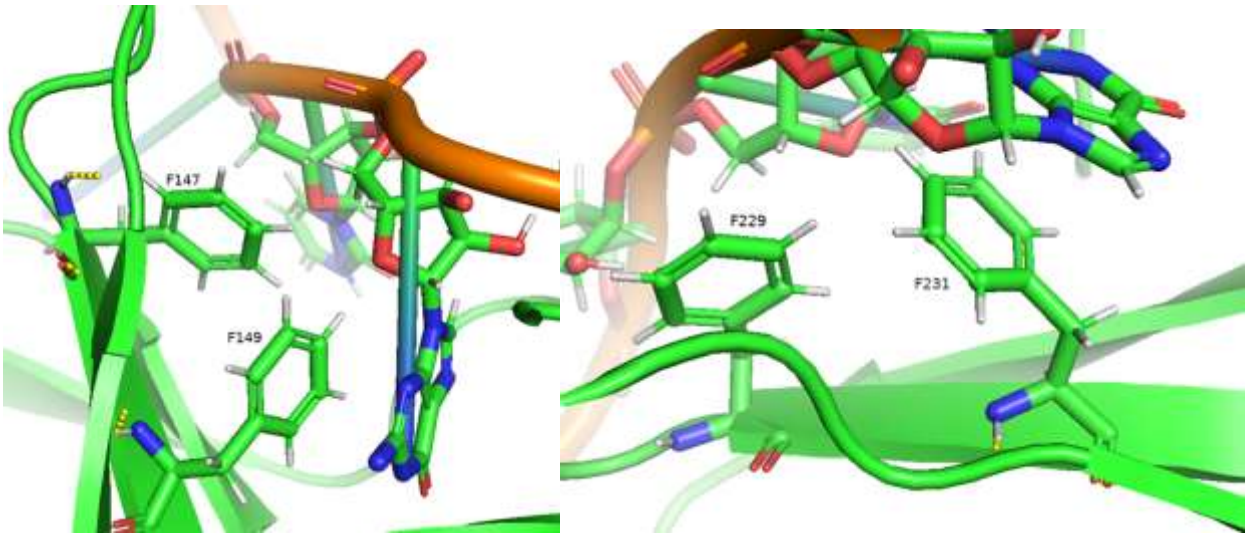

[Figure 20: Left- F147/F149 forming pi-stacking interactions with RNA bases, and hydrogen-bonds with nearby beta-sheet residues. Right- F229/F231 forming pi-stacking interactions with RNA bases, and hydrogen-bonds with nearby beta-sheet residues. PID: 4BS2]

While P112H has been utilized in anisosome studies previously[4], and has been implicated in Frontotemporal Dementia[29,30], structural analysis of P112 did not yield many direct RNA interactions. P112 resides in a heavily disordered loop region that does not bind RNA [Figure 21]. It has been demonstrated that P112H in a RRM1 truncated TDP-43 protein induces a conformational change that disrupts the pi-stacking interactions of W113 with RNA[30]. When observing anisosome phenotype during the experiments, the mutant was shown to have little tendency to form anisosomes; similar to the wild-type protein. This is consistent with the previously mentioned paper demonstrating a reduced tendency for the mutant to aggregate. However, this study was performed with a truncated protein, and it has been shown that the NTD

and CTD of TDP-43 are necessary for significant oligomerization to occur[5]. The lack of anisosome formation may suggest that the mechanism of pathology for P112H does not involve anisosome formation.

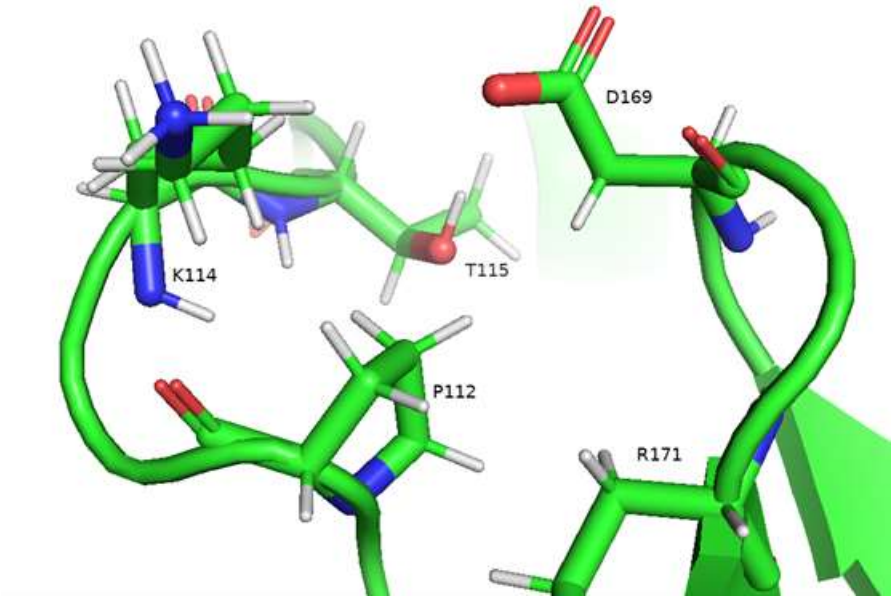

[Figure 21: P112 in a disordered loop region of TDP-43. Nearby residues include K114, T115, D169, and R171. PID: 4BS2]

K263 is similar in position to K181, except that it lies closer to RRM2 than it does RRM1 [Fig. 22]. While no literature binding assays have been performed for this mutant, its structural similarity to K181 and the displayed anisosome phenotype indicates that it likely has significantly reduced RNA-binding affinity.

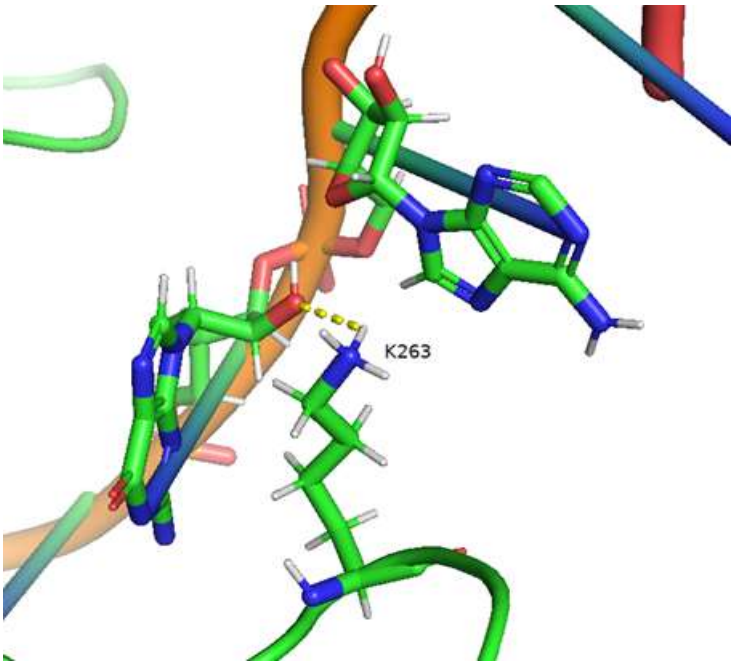

[Figure 22: K263 forming a hydrogen-bond with RNA sugar-phosphate backbone. PID: 4BS2.]

The localization studies of TDP-43 with other nuclear bodies did not yield any significant findings. Previous studies have indicated an overlap of TDP-43 with SC35 and PML bodies,[31] and this was demonstrated to a degree in this thesis. TDP-43 has been implicated as a "bridge" protein between several nuclear bodies. This means that while TDP-43 may not co-localize with a nuclear body, it may still be in association with it. Due to limited time in the lab from the COVID-19 pandemic and other external administrative factors, localization studies were unable to produce any conclusive findings. There may be a lead with SFPQ, but until the discrepancy of its phenotype is faithfully resolved, it cannot be said with certainty that SFPQ interacts with anisosomes. To resolve these discrepancies, future experiments should aim to alter antibody concentration to discern any differences in phenotype. Insights gained from these experiments will provide more data in TDP-43's localization within the cell and will develop our understanding of concentration-dependent

antibody observations. Future experiments should also employ multiple secondary antibodies such that a mosaic of the overexpressed TDP-43 in association with nuclear bodies may be created.

Fluorescent imaging of TDP-43 anisosomes in HEK293T cells allowed for the quantification of anisosome characteristics including propensity, diameter, and granules per nucleus. These quantifications and guides may be used by future research groups when attempting to study multitudes of anisosome phenotypes. The extensive literature search, structural analyses, and phenotype characterizations of TDP-43 anisosomes highlights the importance of structural stability in the propensity of anisosomes. Further evidence should be collected regarding this importance; molecular dynamics simulations and calorimetric assays should be performed to quantify the structural stability of the mutants studied.

Oligomerization and aggregation of proteins is driven by the stability achieved through the formation of thermodynamically favorable interactions. RNA-binding has been shown to stabilize the structure of TDP-43; the loss of RNA destabilizes the protein and allows continued opportunity for conformational perturbations to lead to more favorable interactions found in aggregates. An hypothesis may be that the major driving force of anisosome formation because of binding deficiency is a result of conformational changes associated therewithin. This may also explain why mutated residues that induced conformational changes were more likely to have higher anisosome propensity. The exception to this is K181E, which demonstrates that conformational changes may not be necessary anisosome formation— while a conformational change may be a major driving force, it is not the only factor.

The exact structures of protein aggregates and oligomers are still difficult to discern, as the high electron densities and varying structures of aggregates provide too much noise for data to be reasonably interpreted. As protein visualization techniques and instruments become more

sophisticated, additional support for this hypothesis may be provided. The exact bond formation and arrangements by which these proteins aggregate may eventually be discerned; an hypothesis may be that the mutations either expose internal hydrophobic residues by causing protein misfolding, or oligomerize through interfaces strengthened by the mutations and are present when RNA is not blocking the binding site.

The hypothesis that anisosomes are correlated to disease-causing mutations was further supported in this thesis. Nearly all the mutations that are present in patients with ALS formed anisosomes. However, some of them (P112H, K181A) did not form extensive or robust oligomers. This suggests a few possibilities: (1) anisosomes are involved in the mechanism of disease progression, but do not need to be robust for pathologic outcomes, or (2) that the true mechanism of disease progression is not entirely explained by the formation of anisosomes in vivo. The true answer is likely a combination of these and would require the testing for the presence of endogenous anisosomes in patients through cross-sectional analysis of neuronal tissue, or post-mortem analysis. Additionally, this thesis does not characterize the cytotoxicity of these mutants. All cells were fixed prior to characterization; toxicity assays must be performed to adequately draw this conclusion. While the cells were able to survive for transfection to occur, it is unknown the timescale that is required for anisosomes to be cytotoxic, and toxicity may occur beyond the 24-hour incubation period. Finally, because fluorescence microscopy does not provide information regarding the molecular structure of the anisosomes, it cannot be said with certainty that each "anisosome" signal was a true anisosome. Some may have been insoluble aggregates. Future structural studies must be performed to make such a characterization.

TDP-43 has only become a protein of interest within the past decade or so. The revealing of protein aggregation as a source of cytotoxicity and neurodegeneration only solidifies the need for the

knowledge of the formation of aggregates. It has been shown that aggregation can occur as proteins misfold, but in the case of TDP-43, it often can be caused by the inability to bind stabilizing molecules. Our developing understanding of the driving forces behind the liquid-liquid phase separation of proteins is crucial to develop future therapies for specific pathologies. Understanding this process in thermodynamic terms can lead us to understand the main driving forces behind LLPS. The studies reviewed throughout the process of drafting this paper have made considerable strides in our understanding, but they (including this thesis) fall short in several areas. For instance, several papers lack conformational studies in tandem with the mutants and provide only conjectural conclusions about the molecular effects of binding deficiency. The highly dynamic and prion-like domains of TDP-43 make these conformational studies difficult, and severely hinder the possibility for X-Ray crystal structures to be obtained. Future experiments should seek to subject these mutants to molecular dynamics simulations, as they could provide a possible visual medium for the process of oligomerization. Additionally, no studies were found that displayed the binding energetics for these specific mutations; evidence that would be greatly beneficial to support these hypotheses. Based on the material presented, these hypotheses hold merit and are based within the current scientific understanding, but they must be supported with vigorous evidence. With the data and hypotheses presented in this project, the direction of future studies should follow these suggestions, as they will lead to deeper understanding of the driving forces of LLPS and aid in future developments for the prevention of protein aggregation in neurodegenerative disorders.

Appendix A

Supplemental Information

S1: Immunofluorescence protocol

Materials-

- 4% Formaldehyde – Prepared in 1X PBS
- 1X PBS – (137mM NaCl, 2.7mM KCl, 10mM Na_2HPO_4, 1,8mM KH_2PO_4 at pH 7.4).
- 0.5% Triton-X 100 – Prepared in 1X PBS.
- 3% BSA (Heat Shock Treated) – Prepared in 1X PBS.
- Antibodies – primary and secondary antibodies
- Microscope slides & coverslips
- Mounting media – vector shield mounting media (with DAPI)

Procedure-

1. Put coverslips in 6-well plate and seed cells into the well ($4.5x10^5$ cells/well) 24 hours prior to the experiment.
2. Check for confluency and the healthiness of the cells. Proceed with transfection
3. Stop the reaction by fixing cells with 4% formaldehyde at room temp for 20 min. Wash the cells with 1.5 mL 1X PBS three times and leave the third PBS wash in the well.
4. Aspirate out 1X PBS from the plate and add in 1.5 mL 0.5% Triton-X 100 solution to each well. Incubate for 10 min at room temperature.
5. Dump out Triton solution and wash wells with 1.5 mL 1X PBS for 5 min three times.
6. Decant out 1X PBS solution and add in 1.5 mL 3% BSA. Incubate at room temp for 1 hour.

7. Upon completion of blocking. Cut out a piece of parafilm (3x2 squares) and dispense six 90 μL 1° Ab in 3% BSA solution [say 6 samples are immunostaining for Ab with 1:200 dilution, then it requires 3 μL 1° Ab + 597 μL 3% BSA] onto the clean side of the parafilm.
8. Transfer the coverslip containing cells to a droplet of 1° Ab, cell side facing down. Repeat this process until all the coverslips are transferred onto the parafilm. Incubate the coverslips with 1° Ab at room temp for 1 hr.
9. Wash the coverslips three times (cell side up) with 1.5 mL 1X PBS for 10 min in the 6-well plate on the shaker.
10. Prepare 2° Ab in 3% BSA as described in step 7, and transfer the coverslips as described in step 8. Incubate in the dark at room temp for 1 hr.
11. Wash the coverslips three times with 1.5 mL 1X PBS for 10 min in the dark at room temp on shaker.
12. Place the coverslip onto a microscope slide with a drop of mounting media. Repeat this step until all coverslips are mounted. Leave the slides in the dark at room temp for 10 min.
13. Get rid of excess mounting media.
14. Seal the coverslip with transparent nail polish. Leave the slides in the dark to dry.
15. Visualize it with fluorescence microscope or store in the dark for future analysis.

S2: Transfection Protocol

1. Seat $4x10^5$ cells in a 2cm 6-well plate and incubate at 37°C for 24 hours
2. Incubate transfection mix (100 μL Opti-MEM; 2 μL X-reme Gene 9 Transfection reagent; 1 μg plasmid) in the dark for 30 minutes.
3. Remove 1 mL of media from cells and replace with OG-GFP (1 mL, 0.5 μM in DMEM)
4. Add transfection mix to the cells drop-wise. Incubate for 24 hours

Bibliography

1. Taylor, J. P., Hardy, J., and Fischbeck, K. H. (2002) Toxic proteins in neurodegenerative disease, Science 29

2. Hyman, A. A., Weber, C. A., Julicher, F. (2014) Liquid-Liquid Phase Separation in Biology. *Annu. Rev. Cell Dev. Biol. 30*, 39-58.

3. Babinchak W. M., Surewicz, W. K. (2020) Liquid-Liquid Phase Separation and Its Mechanistic Role in Pathological Protein Aggregation. *Journ. Mol. Biol. 432*, 1910-1925.

4. Yu, H. et al. (2021) HSP70 Chaperones RNA-free TDP-43 into Anisotropic Intranuclear Liquid Spherical Shells. *Science 371,* 585-600.

5. Carter, G. C., Hsiung, C., Simpson, L., Yang, H., Zhang, X. (2021) N-Terminal Domain of TDP-43 Enhances Liquid-Liquid Phase Separation of Globular Proteins. *Journ. Mol. Biol. 433*. 6, 1991-1995.

6. Alberti, S., Gladfelter, A., Mittag, T. (2019) Considerations and Challenges in Studying Liquid-Liquid Phase Separation and Biomolecular Condensates. *Cell 176*, 419-434.

7. Cohen, J. T., et al. (2015) An acetylation switch controls TDP-43 function and aggregation propensity. *Nat Commun 6,* 5845 (2015).

8. Lukavsky, P.J., Daujotyte, D., Tollervey, J.R., Ue, J., Stuani, C., Buratti, E., et al. Molecular basis of UG-rich RNA recognition by the human splicing factor TDP-43. *Nat. Struct. Mol. Biol*., *20*, 1443–1449. (2013).

9. B.S. Johnson, D. Snead, J.J. Lee, J.M. McCaffery, J. Shorter, A.D. Gitler, TDP-43 is intrinsically aggregation prone, and amyotrophic lateral sclerosis-linked mutations accelerate aggregation and increase toxicity. *J. Biol. Chem. 284*, (2009).
10. Johnson, B.S., McCaffery, J.M., Lindquist, S., Gitler, A.D. A yeast TDP-43 proteinopathy model: Exploring the molecular determinants of TDR-43 aggregation and cellular toxicity. *P. Natl. Acad. Sci. U.S.A., 105*, 6439–6444. (2008).
11. Afroz, T., Hock, E.M., Ernst, P., Foglieni, C., Jambeau, M., Gilhespy, L.A.B., et al. Functional and dynamic polymerization of the ALS-linked protein TDP-43 antagonizes its pathologic aggregation. *Nat. Commun., 8, 45.* (2017).
12. Chang, C.K., Wu, T.H., Wu, C.Y., Chiang, M.H., Toh, E.K., Hsu, Y.C., et al. The N-terminus of TDP-43 promotes its oligomerization and enhances DNA binding affinity. *Biochem. Biophys. Res. Commun., 425*, 219–224. (2012).
13. Kuo PH, Chiang CH, Wang YT, Doudeva LG, Yuan HS. The crystal structure of TDP-43 RRM1-DNA complex reveals the specific recognition for UG- and TG-rich nucleic acids. *Nucleic Acids Res. 42*. 4712-4722 (2014).
14. M, McLoughlin C, King A, Smith BN, Troakes C, Pastore A, Shaw CE. RRM adjacent TARDBP mutations disrupt RNA binding and enhance TDP-43 proteinopathy. *Brain. 142,* 3753-3770. (2019).
15. Wang, P., Wander, M. C., Yuan, C., Bereman, M. S., Cohen, T. J. Acetylation-induced TDP-43 pathology is suppressed by an HSF1-dependent chaperone program. *Nat. Commun. 8, 82.* (2017)
16. Workman, R. J., Pettitt, B. M. Thermodynamic Compensation in Peptides Following Liquid-Liquid Phase Separation. *Journ. Phys. Chem. 125*, 6431-6439. (2021)

17. Chen, Y., Cohen, T.J. Aggregation of the nucleic acid-binding protein TDP-43 occurs via distainct routes that are coordinated with stress granule formation. *J. Biol. Chem. 294,* 3696-3706. (2019)
18. Flores, B.N., Li, X., Malik, A. M., Martinez, J., Beg, A. A., Barmada, S. J. An intramolecular Salt Bridge linking TDP-43 RNA Binding, Protein Stability, and TDP43-Dependent Neurodegeneration. *Cell Rep. 27,* 1133-1150. (2019)
19. Buratti, E., Baralle, E. Characterization and Functional Implications of the RNA binding properties of nuclear factor TDP-43, a novel splicing regulator of CFTR Exon 9. *Journ. Biol. Chem. 276,* 36337-36343. (2001)
20. Prasad, A., Bharathi, V., Sivalingam, V., Girdhard, A., Patel, B. K. Molecular Mechanisms of TDP-43 misfolding and pathology in amyotrophic lateral sclerosis. *Front. Mol. Neurosci. 12*. (2019)
21. Zhao, M., Kim, J. R., Bruggen, R., Park, J. RNA-binding proteins in amyotrophic lateral sclerosis. *Mol. Cells. 41,* 818-829. (2018)
22. Lindt, J. V., Bratek-Skicki, A. et al. A generic approach to study the kinetics of liquid-liquid phase separation under near-native conditions. *Commun. Biol. 4.* (2021)
23. Sreedharan, J., et al. TDP-43 mutations in familial and sporadic amyotrophic lateral sclerosis. *Science. 319.* (2008)
24. Ayala, Y. M. et al. Structural Determinants of the cellular localization and shuttling of TDP-43. *Journ. Cell Science. 121,* 3778-3785. (2008)
25. Francois-Moutal, L., Perez-Miller, S. et al. Structural Insight into tdp-43 and effects of post-translational modifications. *Front. Mol. Neurosci. 12,* (2019)

26. Kuo, PH., et al. Structural insights into TDP-43 in nucleic-acid binding and domain interactions. *Nucleic Acid Res. 37,* 1799-1808. (2009)

27. Weskamp, K., Barmada, S. J. TDP43 and RNA instability in amyotrophic lateral sclerosis. *Brain Res. 1693,* 67-74. (2018)

28. Rengifo-Gonzalez, J. C., et al. The cooperative binding of TDP43 to GU-rich RNA repeats antagonizes TDP-43 aggregation. *eLife, 10.* (2021).

29. Agrawal, S., et al. Frontotemporal dementia-linked P112H mutation of TDP-43 induces protein structural change and impairs its RNA binding function. *Protein Science. 30,* 350-365. (2020).

30. Moreno, F., et al. A novel mutation P112H in the TARDBP gene associated with frontotemporal lobar degeneration without motor neuron disease and abundant neuritic amyloid plaques. *Acta Neuro. Commun. 3.* (2015).

31. Sephton, C. F., et al. TDP-43 in CNS development and function: clues to TDP-43-associated neurodegeneration. *Biol. Chem. 393.* 589-594 (2012).

32. Zhang, L.; Wang, L.; Kao, Y. -T.; Qiu, W.; Yang, Y.; Okobiah, O.; Zhong, D. Mapping hydration dynamics around a protein surface. *Proceedings of the National Academy of Sciences*. ***3.*** 18461–18466. (2007).

33. Dill, K. A. The protein-folding problem, 50 years on. *Science*. ***338***. 1042–1046

34. Dee, D. R.; Woodside, M. T. Comparing the Energy Landscapes for Native Folding and Aggregation of PrP. *Prion*. *10*. 207-220. (2016)

ACADEMIC VITA

Eli Mertick-Sykes

Department of Biochemistry and Molecular Biology

The Pennsylvania State University

Education:

June 2018 - Present B.S. Student, Biochemistry and Molecular Biology (major)
The Pennsylvania State University, University Park, PA

Professional Experience:

Sept. 2019 – Present Undergraduate Research Assistant, Advisor; Dr. Xin ZhangChemistry Department, The Pennsylvania State University

Research Projects: Degradation of Protein Aggregates via Small Molecule Activation ofAutophagy.

- Worked with cell cultures to determine several compounds' effectiveness of clearing protein aggregates.
- Used light, and fluorescence microscopy to visualize proteins in vivo.
- Received several awards/grants for research.
- Presented methodology at Undergraduate Research Poster Exhibition

Understanding Folding States of RNA-Binding Proteins in Membraneless Organelles.

- Studied the tendency of protein TDP-43 to aggregate under stress in livecells.

Honors Thesis- The Colocalization of Anisosome-forming RNA-binding Deficient TDP-43 with Nuclear Proteins and Bodies

- Researched the exciting and rising area of liquid-liquid phase separation.
- Used Immunostaining and immunofluorescence to visualize and characterize RNA-Binding deficient TDP-43 phase-separated granules (anisosomes) in HEK293T Cells.
- Characterized several TDP-43 mutants in their ability to form anisosomes.

Jan. 2022— Present General Biochemistry Teaching Assistant/Grader

Aug. 2021— Present Organic Chemistry Laboratory Teaching Assistant

- Taught 16 students per semester several fundamental organic laboratory practices.

- Analytical, spectral, and purification techniques include Liquid-Liquid extraction using acid/base chemistry, preparing, obtaining, and interpreting NMR/IR spectral data, distillation, column chromatography, and recrystallization.

- Facilitated safe lab practices, taught the importance of being a conscientious lab partner, and performed routine demonstrations of lab techniques.

Jan. 2021 – May 2021 Physical Chemistry: Thermodynamics Teaching Assistant

- Taught 30+ students the fundamentals and key interpretations of thermodynamics
  - Understanding and interpretations of engine cycles, phase diagrams, solution chemistry, calorimetry, gas laws, and electrochemistry.
  - Derivations and interpretations of mathematical functions such as entropy, enthalpy, the Gibbs' potential, etc. and their applications in chemical reactions and the characterization of equilibrium states,
- Given an average rating of 6/7 on Student Rating of Teaching Effectiveness

Jan. 2020 – Present Organic Chemistry Teaching Assistant

- Taught 100+ students per semester the fundamentals of organic chemistry including organic structure, acid-base chemistry, NMR and IR spectroscopy, Mass Spectrometry, substitution/elimination reactions, organic synthesis, and radical/polymerization reactions.
- Given an average rating of 6.2/7 on Student Rating of TeachingEffectiveness

Jan. 2020 – Present Chemistry Grader

Honors and Awards:

Dec. 2021 George E., Jr. and Elizabeth S. Sperling Tutorial Endowment in Calculus, Physics, Chemistry and Mathematics

Nov. 2021 Learning Assistant Excellence Scholarship

June 2020 Erickson Discovery Grant

- Awarded for research on the Degradation of Protein Aggregates viaSmall Molecule Activation of Autophagy.

May 2020 Eberly College of Science Summer Undergraduate Research Award

- Awarded for research on the Degradation of Protein Aggregates viaSmall Molecule Activation of Autophagy.

June 2020 —Present Schreyer Honors College

Dec. 2018 – Present Dean's List

Work Experience:

July 2017 – July 2020 Cashier, Wegmans approx. 15 hours per week

Additional Relevant Skills:

- Presented Research at Poster Exhibition
- Plasmid Design/Molecular Cloning
- Use of Bioinformatics tools such as BLAST, Clustal, SnapGene, and PyMOL
- Chemical Hazardous Waste Training
- 1D and 2D-Nuclear Magnetic Resonance and Infrared Spectroscopy
- Mass Spectrometry
- Common biochemical laboratory techniques including Mini/Midi-Prep, Gel Electrophoresis, Column Chromatography, Mammalian Tissue Culture Maintenance, Fluorescence microscopy, and Antibody preparation.